Reactive astrocytes promote proteostasis in Huntington's disease through the JAK2-STAT3 pathway

Laurene Abjean, Lucile Ben Haim, Miriam Riquelme-Perez, Pauline Gipchtein, Céline Derbois, Marie-Ange Palomares, Fanny Petit, Anne-Sophie Hérard, Marie-Claude Gaillard, Martine Guillermier, et al.

HAL Id: cea-03872742
https://cea.hal.science/cea-03872742

Submitted on 25 Nov 2022

Reactive astrocytes promote proteostasis in Huntington's disease through the JAK2-STAT3 pathway

Laurene Abjean,[1] Lucile Ben Haim,[1,†] Miriam Riquelme-Perez,[1,2,†] Pauline Gipchtein,[1] Céline Derbois,[2] Marie-Ange Palomares,[2] Fanny Petit,[1] Anne-Sophie Hérard,[1] Marie-Claude Gaillard,[1] Martine Guillermier,[1] Mylène Gaudin-Guérif,[1] Gwennaëlle Aurégan,[1] Nisrine Sagar,[1] Cameron Héry,[1] Noëlle Dufour,[1] Noémie Robil,[3] Mehdi Kabani,[1] Ronald Melki,[1] Pierre De la Grange,[3] Alexis P. Bemelmans,[1] Gilles Bonvento,[1] Jean-François Deleuze,[2] Philippe Hantraye,[1] Julien Flament,[1] Eric Bonnet,[2] Solène Brohard,[2] Robert Olaso,[2] Emmanuel Brouillet,[1] Maria-Angeles Carrillo-de Sauvage[1] and Carole Escartin[1]

1 Université Paris-Saclay, Commissariat à l'Energie Atomique et aux Energies Alternatives, Centre National de la Recherche Scientifique, MIRCen, Laboratoire des Maladies Neurodégénératives, 92265, Fontenay-aux-Roses, France

2 Université Paris-Saclay, Commissariat à l'Energie Atomique et aux Energies Alternatives, Centre National de Recherche en Génomique Humaine, 91057, Evry, France

3 GenoSplice technology, 75013 Paris, France

Correspondence to: Carole Escartin, PhD

UMR9199 - MIRCen

CNRS - CEA - Université Paris Saclay

18, route du Panorama

92260 Fontenay-aux-roses, France

E-mail: carole.escartin@cea.fr

[†]**These authors contributed equally to this work.**

Running title: STAT3-mediated proteostasis in HD astrocytes

Abstract

Huntington's disease is a fatal neurodegenerative disease characterized by striatal neurodegeneration, aggregation of mutant Huntingtin and the presence of reactive astrocytes.

Astrocytes are important partners for neurons and engage in a specific reactive response in Huntington's disease that involves morphological, molecular and functional changes. How reactive astrocytes contribute to Huntington's disease is still an open question, especially because their reactive state is poorly reproduced in experimental mouse models.

Here, we show that the JAK2-STAT3 pathway, a central cascade controlling astrocyte reactive response, is activated in the putamen of Huntington's disease patients. Selective activation of this cascade in astrocytes through viral gene transfer reduces the number and size of mutant Huntingtin aggregates in neurons and improves neuronal defects in two complementary mouse models of Huntington's disease. It also reduces striatal atrophy and increases glutamate levels, two central clinical outcomes measured by non-invasive magnetic resonance imaging. Moreover, astrocyte-specific transcriptomic analysis shows that activation of the JAK2-STAT3 pathway in astrocytes coordinates a transcriptional program that increases their intrinsic proteolytic capacity, through the lysosomal and ubiquitin-proteasome degradation systems. This pathway also enhances their production and exosomal release of the co-chaperone DNAJB1, which contributes to mutant Huntingtin clearance in neurons.

Together, our results show that the JAK2-STAT3 pathway controls a beneficial proteostasis response in reactive astrocytes in Huntington's disease, which involves bi-directional signalling with neurons to reduce mutant Huntingtin aggregation, eventually improving disease outcomes.

Abbreviations: AAV = Adeno-Associated Virus; DARPP32 = Dopamine- and cAMP-Regulated neuronal Phosphoprotein; BSA = Bovine Serum Albumin; DNAJB1 = DnaJ heat shock protein family (Hsp40) member B1; FACS = Fluorescence-Activated Cell Sorting; GFAP = Glial Fibrillary Acidic Protein; Glutamate Chemical Exchange Saturation transfer = gluCEST; HBSS = Hank's Balanced Salt Solution; HSP = Heat Shock Proteins; JAK = Janus Kinase; LV = Lentiviral Vector; mHTT = mutant Huntingtin; RT = Room Temperature; SDS = Sodium Dodecyl Sulfate; SOCS3 = Suppressor Of Cytokine Signalling 3; STAT3 = Signal Transducer and Activator of Transcription 3; Tx = Triton X-100; Ub = Ubiquitin; UPS = Ubiquitin-Proteasome System; WT = Wild type.

Introduction

Huntington's disease is a genetic neurodegenerative disease that causes involuntary movements, psychiatric symptoms and cognitive deficits, with no curative treatment yet available[1]. Huntington's disease is caused by an expansion of CAG triplet repeats in the *Huntingtin* (*HTT*) gene, leading to an abnormal polyglutamine tract in the N-terminal part of the protein HTT[2]. Both loss and gain of function of HTT contribute to the dysfunction and death of projection neurons in the caudate/putamen (striatum in mice) and cerebral cortex. A key neuropathological hallmark of Huntington's disease is the presence of mutant HTT (mHTT) aggregates, primarily in neurons[3], but also in glial cells[4, 5]. In the brain of Huntington's disease patients, astrocytes progressively become reactive, which was initially characterized by their hypertrophic morphology and overexpression of Glial Fibrillary Acidic Protein (GFAP)[6-8]. Reactive astrocytes also display significant changes in gene expression in the putamen[9] and cortex[5] of Huntington's disease patients. Astrocytes are essential partners of neurons, as they perform many key functions including metabolic and trophic support, antioxidant defence and regulation of synaptic transmission and plasticity[10]. How are these functions changed in Huntington's disease? Most studies report defective astrocyte functions in Huntington's disease models[11], including reduced glutamate uptake[12], altered K$^+$ buffering[13], impaired regulation of blood flow[14], as well as reduced synthesis and release of antioxidants[15], trophic factors[16], gliotransmitters[17] and exosomes[18]. However, in most cases, Huntington's disease mouse models poorly replicate the reactive state of astrocytes observed in Huntington's disease human brains, based on GFAP overexpression, hypertrophy[11, 13] and transcriptional profile, as recently captured with genome-wide transcriptomic analysis[9, 19, 20]. Therefore, the impact of reactive astrocytes on disease progression is still unclear.

The Janus Kinase (JAK)-Signal Transducer and Activator of Transcription 3 (STAT3) pathway is a central cascade controlling astrocyte reactive response[21]. STAT3 activation is found in reactive astrocytes of genetic models of Huntington's disease in mice and non-human primates[22]. However, it is still unknown whether this pathway is also activated in reactive astrocytes observed in Huntington's disease patients and which astrocyte functions are regulated by this pathway.

We previously reported that inhibition of the JAK2-STAT3 pathway in reactive astrocytes in

1 an acute model of Huntington's disease reduces their reactive features and increases the number

2 of mHTT aggregates[22]. mHTT aggregates are mainly composed of N-terminal fragments of

3 mHTT, which trap several important proteins such as transcription factors or chaperones[23, 24] and

4 generate deleterious steric hindrance. However, aggregates may also contribute to remove toxic

5 soluble mHTT from the cytosol[25]. Soluble mHTT can be degraded by the Ubiquitin-Proteasome

6 System (UPS), while aggregates can only be cleared by autophagy coupled to lysosomal

7 degradation[26, 27]. Astrocytes are reported to have high proteolytic capacity, including for mHTT,

8 which could explain why fewer aggregates are observed in astrocytes than in neurons[28, 29]. Yet, it

9 is unknown whether the UPS and autophagy/lysosome systems are specifically altered in

10 Huntington's disease astrocytes[30, 31], and how these systems can be stimulated in astrocytes to

11 promote mHTT clearance. Another important proteostasis mechanism preventing mHTT

12 aggregation is operated by chaperones, which promote HTT proper folding, prevent abnormal

13 interactions with cellular proteins and guide mHTT to degradation systems[32, 33]. In particular,

14 Heat Shock Proteins (HSP) prevent mHTT aggregation in different cell types[32, 34].

15   Here, we studied how the JAK2-STAT3 pathway controls astrocyte reactive response in

16 Huntington's disease, focusing on their ability to promote cellular proteostasis. We observed

17 STAT3 activation in reactive astrocytes in the brain of Huntington's disease patients. In two

18 complementary mouse models of Huntington's disease, we found that activation of the JAK2-

19 STAT3 pathway in reactive astrocytes reduces both the number and size of mHTT aggregates in

20 neurons, without increasing soluble mHTT levels, and improves several disease hallmarks.

21 Genome-wide transcriptomics and functional analysis showed that JAK2-STAT3 pathway

22 activation induces a specific proteostasis signature in astrocytes associated with higher

23 proteolytic activity. It also induces astrocyte expression of the co-chaperone DNAJB1, which is

24 loaded in exosomes and reduces mHTT aggregation in neurons. Our results show that the JAK2-

25 STAT3 pathway controls a bi-directional communication between reactive astrocytes and

26 neurons in Huntington's disease, which eventually reduces mHTT aggregation and improves

27 neuronal alterations.

28 # Materials and methods

29 ## Mice

30   Heterozygous knock-in mice (Hdh140 mice) expressing a chimeric mouse/human exon 1

containing 140 CAG repeats inserted into the murine *Htt* gene on a C57BL/6J background were originally obtained from the Jackson laboratory (stock # 027409)[35]. Male and female Hdh140 mice and their littermate controls were injected with different viral vectors (see below) at 7-10 months and euthanized 4 months later. Wild type (WT), adult male C57BL/6J mice were injected at 2.5 months of age, with different viral vectors and euthanized 1.5 months later.

All experimental protocols were reviewed and approved by the local ethics committee (CETEA N°44) and the French Ministry of Education and Research (Approval APAFIS#4554-2016031709173407). They were performed in an authorized animal facility (authorization #D92-032-02), in strict accordance with recommendations of the European Union (2010-63/EEC), and in compliance with the 3R guidelines. Animal care was supervised by a dedicated veterinarian and animal technicians. Mice were housed in groups of 5, under standard environmental conditions (12-hour light-dark cycle, temperature: $22 \pm 1°C$ and humidity: 50%) in filtered cages, with *ad libitum* access to food and water.

Viral vectors

We either used lentiviral vectors (LV) or adeno-associated vectors (AAV) to drive transgene expression in neurons or in astrocytes, as described in each figure.

Self-inactivated LV were produced by transient co-transfection of 293T cells with four plasmids encoding viral structural proteins, the envelope protein and the transgenic cDNA under the control of a phosphoglycerate kinase 1 promoter and followed by the woodchuck hepatitis virus post-transcriptional regulatory element, to enhance transgene expression[36]. To target neurons, LV were pseudotyped with the G-protein of the vesicular stomatitis virus[37]. To target astrocytes, LV were pseudotyped with the rabies-related Mokola envelope and lentiviral recombinant genome contained four repeats of the miR124 target to repress transgene expression in neurons[36]. LV are referred to as "LV_A- or LV_N-name of the transgene" depending the cell type targeted: A for astrocytes and N for neurons. Lentiviral particle titers were determined by ELISA quantification of the nucleocapsid p24 protein.

AAV (AAV2, serotype 9) contain the gfaABC1D promoter, a synthetic promoter derived from the GFAP promoter[38], and transduce astrocytes. AAV were produced according to validated procedures[39]. Viral genome concentration was determined by qPCR on DNase resistant particles.

1 Viral vectors encoding murine *Socs3* or *Jak2^{T875N}*, a constitutively active form of JAK2

2 (JAK2ca), were used to respectively, inhibit or activate the JAK2-STAT3 pathway in mouse

3 astrocytes[22, 39, 40]. They were co-injected with a viral vector encoding the fluorescent proteins *Gfp*

4 or *Td-Tomato* to visualize transduced cells (same total viral load). For some experiments, the

5 same viral vectors were injected in both striata. For other experiments, each striatum of the same

6 mouse received different viruses and data were analysed with paired statistical tests.

7 LVs encoding the first 171 N-terminal amino acids of human *Huntingtin* (*HTT*) cDNA with

8 82 polyglutamine repeats that target either striatal neurons [LV$_N$-mHTT[41]] or astrocytes [LV$_A$-

9 mHTT[8]] were used as LV-based models of Huntington's disease.

10 Last, we generated LV$_A$ expressing full-length human *DNAJB1* (LV$_A$-DNAJB1) or the

11 dominant negative mutant corresponding to the J-domain of human *DNAJB1*[42] [LV$_A$-DNAJB1-

12 DN]. The initial cDNA was generated by GeneArt Gene Synthesis services (Invitrogen,

13 Carlsbad, CA) based on published sequences, and inserted into a pENTR® transfer plasmid.

14 Gateway® recombination (Thermofisher Scientific) was used to clone these cDNA into

15 appropriate self-inactivated LV expression plasmid containing the phosphoglycerate kinase 1

16 promoter, the woodchuck hepatitis virus post-transcriptional regulatory element and four

17 miR124 target sequences.

Immunostaining quantification

19 Levels of GFAP immunoreactivity and GFAP$^+$ volumes were quantified on 10x-tiled images

20 of serial sections along the antero-posterior axis of the striatum, acquired with an epifluorescence

21 microscope (Leica DM6000, Nussloch, Germany). Virally transduced GFP$^+$ area was manually

22 segmented on each section and the corresponding mean intensity signal for GFAP in this area

23 was extracted with Image J. Background intensity signal was measured on unstained regions of

24 the same section and subtracted to the GFAP total signal. The volume was calculated from the

25 area measured on each section by the Cavalieri method[40].

26 To quantify lesion size, images of DARPP32 immunostained serial striatal sections were

27 acquired at the 5x objective with an epifluorescence microscope (Leica DM6000). DARPP32-

28 depleted area in the striatum was manually segmented with Image J on each serial section, and

29 the total volume calculated with the Cavalieri method.

To quantify astrocyte soma area and STAT3 immunoreactivity, stacked confocal images of GFP and STAT3 immunostained sections were acquired with a 40× objective (three brain sections per mouse, three fields per section, 10 to 16 z-steps of 1 μm, maximum intensity stack). GFP[+] cell bodies were manually segmented and their individual area and mean grey value for STAT3 were measured with Image J.

The total number and surface of EM48^{+} and Ubiquitin[+] aggregates were quantified on serial striatal sections along the antero-posterior axis, scanned with an Axio scanZ.1 (Zeiss, Oberkochen, Germany) at the 40× objective in bright field microscopy mode, with multi-plan focusing. Aggregates were automatically detected by the Morphostrider software (ExploraNova), with intensity, size and shape thresholds, after manual segmentation of the striatum on each section. The total number of aggregates within each striatum was then calculated. To quantify the distribution of EM48^{+} aggregates in DARPP32^{+} neurons and GFP[+] astrocytes, stacked confocal images (16 z-steps of 1 μm, maximum intensity stack) were acquired on a Leica TCS SP8 confocal fluorescent microscope with a 40x objective (three brain sections per mouse, three fields per section). Aggregates were automatically detected with ImageJ software, with intensity, size and shape thresholds. Laser intensity, detection settings and analysis parameters were identical between each mouse of the same cohort. The number of aggregates in each cell type and the total number were manually quantified using ImageJ cell counter plugin.

Quantification of cathepsin and proteasome activities in astrocytes

Hdh140 mice previously injected with astrocyte-specific AAV-GFP or AAV-Td-Tomato in the striatum to label astrocytes, were perfused with cold PBS for 4 min. Their striata were rapidly collected in Hank's Balanced Salt Solution (HBSS; Sigma). Cells were mechanically and enzymatically dissociated with fire-polished Pasteur pipettes and the neural tissue dissociation kit with papain (Miltenyi Biotec, Bergisch Gladbach, Germany), following manufacturer's instructions. After filtration through a 50 μm-filter, myelin removal beads II and MS columns (Miltenyi Biotec) were used to deplete myelin from cell suspensions. Cells were then resuspended in 0.5% PNB buffer (Perkin Elmer, FP1020) and incubated for 30 min with 1 μM fluorescent cathepsin probe (iABP, Vergent Bioscience, Minneapolis, MN, #40200) or with 200 nM proteasome probe (UbiQ, Bio BV, Amsterdam, the Netherlands, #UbiQ-018) at RT. Cells were centrifuged at 300 g for 5 min at 4°C and resuspended in 400 μl HBSS. They were sorted

1   on a BD Influx cell sorter. GFP expressed by infected astrocytes was detected at 530/40 nm (488

2   nm excitation) and the cathepsin probe was detected at 670/30 nm (646 nm excitation). Td-

3   Tomato expressed by infected astrocytes was detected at 579/34 nm (561 nm excitation) and the

4   proteasome probe at 530/40 nm (488 nm excitation). Control samples of unlabelled or mono-

5   fluorescent brain cells were used to define detector gains and sorting gates, which were kept

6   constant for all samples. No compensation was required to accurately quantify the two

7   fluorescent signals within the same cell. Cells were gated on a side scatter/ forward scatter plot,

8   then singlets were selected and finally the percentage of GFP$^+$/Cathepsin$^+$ or Td-

9   Tomato$^+$/Proteasome$^+$ astrocytes was quantified in each mouse, after setting the gates on GFP$^+$ or

10   Td-Tomato$^+$ astrocytes incubated without a probe (i.e. "Fluorescence Minus One" controls,

11   **Supplementary Fig. 1B**).

12   Statistics

13   Values for individual samples are shown on graphs. Arithmetic means are represented by a

14   horizontal line and paired samples from two groups are connected by a line. Sample size was

15   chosen based on prior experience to yield adequate power to detect specific effects. Mice of the

16   appropriate genotype were randomly allocated to experimental groups and processed

17   alternatively. Statistical analysis was performed with Statistica software (StatSoft, Tulsa, OK)

18   and graphs were prepared with GraphPad Prism 7 (La Jolla, CA). Paired or unpaired two-tailed

19   Student *t*-test were used to compare two groups, or two-way ANOVA to compare four groups.

20   Normality of residues and homoscedasticity were assessed. If any condition of application was

21   not fulfilled, we used non-parametric tests: two groups were compared by the Mann-Whitney or

22   Wilcoxon matched-pair tests. Percentages were first changed to proportions and transformed by

23   the *arcsine* function, before being analysed by paired or unpaired *t*-test.

24   Investigators were partially blinded to the group when performing experiments and analysis,

25   as the group can be deduced by the presence of aggregates or GFP levels for example. The

26   significance level was set at $p < 0.05$. In each figure legend, N refers to the number of mice.

27   Data availability

28   Microarray datasets are deposited on GEO under reference GSE107486. RNAseq datasets are

29   deposited on GEO under reference GSE171141.

8

Detailed protocols for stereotactic injections, immunohistology, protein extraction, exosome isolation, immunoblot, RNA extraction and RT-qPCR, microarray, RNAseq analysis and identification of transcription factors as well as magnetic resonance imaging are provided as **Supplementary material**.

Results

STAT3 activation in reactive astrocytes in Huntington's disease patients

STAT3 is involved in the control of reactive astrocytes in multiple CNS diseases and corresponding animal models[21], but it has never been studied in the brain of Huntington's disease patients. As the active tyrosine-phosphorylated epitope on STAT3 is poorly preserved in such post-mortem samples, increased nuclear accumulation of total STAT3 is used as a surrogate of its activation[21]. We performed STAT3 immunostainings in the putamen of Huntington's disease patients (Vonsattel grade III[6]) and their age- and sex-matched controls. There was a stronger STAT3 immunoreactivity in Huntington's disease patients (**Fig. 1A, B**), especially in regions showing neurodegeneration, as seen by their lower density in NeuN^{+} neurons and higher density in hypertrophic GFAP[+] astrocytes (**Fig. 1C**). Many STAT3^{+} cells had a typical astrocyte morphology and displayed nuclear accumulation of this transcription factor (**Fig. 1B, C**), an indication of pathway activation.

We also analysed available transcriptomic data of nuclei isolated from the cingulate cortex of grade III/IV Huntington's disease patients[5] to identify potential active transcription factors in Huntington's disease astrocytes. Several bioinformatics tools (based on literature mining or DNA motif recognition in the promoter of differentially expressed genes, see Methods) identified STAT3 as a potential regulatory transcription factor in Huntington's disease astrocytes, with significant associated *p* values (**Supplementary table 1**).

Together, these results support a role for STAT3 in driving astrocyte reactive changes in Huntington's disease.

Astrocytic JAK2-STAT3 pathway reduces neuronal mHTT aggregation in two mouse models of Huntington's disease

9

To determine the molecular and functional regulation operated by STAT3 in Huntington's disease reactive astrocytes, we took advantage of our viral vectors that transduce striatal astrocytes with high efficiency and selectivity (**Supplementary Fig. 1A**), to either activate or inhibit the JAK2-STAT3 pathway[39, 40].

We first studied knock-in Hdh140 mice that express a humanized *HTT* gene with 140 CAG repeats under its own endogenous promoter[35]. These mice develop progressive Huntington's disease symptoms with small intra-neuronal mHTT aggregates, early transcriptional defects in neurons, but very mild morphological and molecular reactive changes in astrocytes[20, 43]. In this model, we thus stimulated the JAK2-STAT3 pathway in striatal astrocytes by virus-mediated expression of a constitutively active form of JAK2 (JAK2ca).

A lentiviral vector targeting astrocytes and encoding JAK2ca (LV$_A$-JAK2ca) was injected in 7-9 month-old heterozygous Hdh140 mice, with a LV$_A$ encoding GFP (LV$_A$-GFP) to visualize infected astrocytes (Hdh140-JAK2ca mice, **Fig. 2A**). Controls were Hdh140 mice injected with LV$_A$-GFP at the same total viral titer (Hdh140-GFP mice), and brains from both groups were analysed 4 months later (**Fig. 2A**). Immunostaining on mouse brain sections showed that JAK2ca activated STAT3 (**Fig. 2B**) and induced the two cardinal features of reactive astrocytes: overexpression of the intermediate filaments GFAP (**Fig. 2B, C**) and soma hypertrophy (**Fig. 2B, D**). JAK2ca also increased mRNA levels of *Vimentin* and *Serpina3n,* two markers of reactive astrocytes (**Fig. 2E, F**). We controlled that JAK2ca did not impact total mRNA levels of murine *Htt* and *mHTT,* which were expressed at similar levels in Hdh140-JAK2ca and Hdh140-GFP groups (Student *t*-test, n = 3-4/group, df = 5, t = 1.367, p = 0.230 and t = 1.276, p = 0.258 respectively, data not shown).

JAK2ca expression in Hdh140 astrocytes significantly reduced the total number of mHTT aggregates in the striatum (**Fig. 2G, H**). The size of EM48$^+$ aggregates was also significantly decreased in Hdh140-JAK2ca mice (**Fig. 2I**). Most EM48$^+$ aggregates were in small neuronal processes, while more than 30% of them were found in the nucleus or cell body of striatal neurons expressing dopamine- and cAMP-regulated neuronal phosphoprotein (DARPP32), and less than 1% of all mHTT aggregates were found in GFP$^+$ astrocytes (**Fig. 2J, K**). Despite the marked reduction in the number of mHTT aggregates, this relative distribution was not significantly impacted by JAK2ca (Student *t*-test on *arcsine*-transformed data, n = 3-4/group, *df*

1   = 5, *t* = 1.983, *p* = 0.104 for DARPP32$^+$ neurons, *t* = 0.517, *p* = 0.627 for GFP$^+$ astrocytes, **Fig.**

2   **2K**).

3   To determine whether soluble mHTT was also reduced by JAK2ca, we analysed Triton X-100

4   (Tx)-soluble protein extracts prepared from the striatum of WT and Hdh140 mice injected with

5   LV$_A$-GFP or LV$_A$-JAK2ca. Immunoblotting with the 1C2 antibody that recognizes preferentially

6   the elongated polyglutamine stretch of mHTT[44] showed similar Tx-soluble mHTT levels in both

7   groups (**Fig. 2L, M**). We then immunoblotted proteins from the Tx-insoluble, SDS-soluble

8   fraction with the 2B4 antibody, which preferentially binds to the N-terminal part of mHTT[45].

9   High molecular weight forms of mHTT corresponding to aggregated fragments of mHTT were

10   detected only in samples from Hdh140 mice. The levels of high molecular weight aggregated

11   mHTT were lower in the Hdh140-JAK2ca group, in accordance with histological data of reduced

12   mHTT aggregation with JAK2ca (**Fig. 2N, O**).

13   We then took advantage of another lentiviral mouse model of Huntington's disease that better

14   replicates the strong neurodegeneration and subsequent astrocyte reactivity observed in patients[8,]

15   [22]. This model involves lentivirus-mediated expression of the 171 first amino acids of human

16   HTT with 82 CAG repeats specifically in striatal neurons[8, 41] (**Fig. 3A**). In this model, we

17   performed the inverse manipulation of the JAK2-STAT3 pathway in astrocytes, by blocking it

18   with its inhibitor Suppressor Of Cytokine Signalling 3 (SOCS3). SOCS3 efficiently blocked

19   STAT3 activation and reactive changes in astrocytes (**Fig. 3B-F**)[22]. Moreover, SOCS3

20   expression in striatal astrocytes increased the aggregation of mHTT in neurons, as seen with

21   EM48 immunostaining (**Fig. 3G, H**). Less than 2% of mHTT aggregates were found in GFP$^+$

22   astrocytes (**Fig. 3H**), and this distribution was not changed by SOCS3 (Student *t*-test on *arcsine*-

23   transformed data, *n* = 6/group, *df* = 5, *t* = 0.917, *p* = 0.401). mHTT aggregates are ubiquitinated

24   and the total number of Ubiquitin (Ub)$^+$ aggregates was also increased by SOCS3 (**Fig. 3I, J**). In

25   addition, aggregates were larger in the SOCS3 group than in the GFP group (**Fig. 3K**), revealing

26   both quantitative and qualitative changes in neuronal mHTT aggregates following JAK2-STAT3

27   inhibition in astrocytes.

28   Activation of JAK2-STAT3 pathway in astrocytes is beneficial for striatal neurons

29   We next evaluated how JAK2-STAT3 pathway activation in astrocytes impacted several

1 disease outcomes. Hdh140 mice do not show the massive striatal neurodegeneration typical of

2 Huntington's disease patients, but they replicate the early transcriptional defects in striatal

3 neurons, in particular for *Ppp1r1b* transcripts (which encode the striatal protein DARPP32). In

4 Hdh140 mice, JAK2ca expression in striatal astrocytes significantly increased levels of the

5 neuronal transcript *Ppp1r1b* (**Fig. 4A**), suggesting a beneficial effect on neurons. To further

6 demonstrate JAK2ca beneficial effects on clinically-relevant pathological outcomes, we next

7 performed magnetic resonance imaging. Eighteen month-old heterozygous Hdh140 mice display

8 significant striatal atrophy[46], likely due to the atrophy of striatal neurons themselves[47], and not to

9 their death, as neuronal loss was described only in older homozygous Hdh140 mice[43]. Striatal

10 volume can be measured accurately with T_2-weighted magnetic resonance imaging[48], and striatal

11 atrophy is observed at prodromal stages in Huntington's disease patients[49]. Hdh140 mice also

12 display lower striatal levels of the major neurotransmitter and metabolic intermediate

13 glutamate[48], again replicating an early pathological hallmark of Huntington's disease patients[50].

14 Brain glutamate distribution can be mapped with a high resolution using glutamate Chemical

15 Exchange Saturation Transfer (gluCEST)[51], revealing local reduction in glutamate abundance in

16 Hdh140 mice[52]. Hdh140 mice were injected in one striatum with LV_A-JAK2ca + LV_A-GFP and

17 the other striatum with LV_A-GFP as an internal control, and imaged 2 months later. The volume

18 of the striatum injected with LV_A-JAK2ca was significantly larger than the contralateral striatum

19 injected with LV_A-GFP (**Fig. 4B**), showing reduced atrophy with JAK2ca. Likewise, gluCEST

20 imaging revealed significantly higher striatal levels of glutamate with JAK2ca (**Fig. 4C**), further

21 supporting beneficial effects of JAK2-mediated astrocyte reactivity on two pathological

22 hallmarks of Huntington's disease.

23 In the lentiviral model, mHTT causes local neuronal degeneration, visible as DARPP32-

24 depleted lesion (**Fig. 4D**). SOCS3 significantly increased the lesion volume (**Fig. 4E**), and

25 reduced *Ppp1r1b* mRNA levels (**Fig. 4F**).

26 Overall, our data show that activation of the JAK2-STAT3 pathway in reactive astrocytes

27 reduces the number and size of mHTT aggregates in neurons and mitigates Huntington's disease

28 neuronal alterations; while blocking the pathway has opposite effects.

JAK2ca regulates the expression of proteostasis genes in astrocytes

30 How can JAK2-STAT3 pathway activation in reactive astrocytes impact mHTT aggregation

1   in neurons? As the JAK2-STAT3 cascade regulates gene expression, we investigated

2   transcriptional changes induced by JAK2ca by comparing the transcriptome of acutely sorted

3   astrocytes isolated from WT-JAK2ca and WT-GFP control mice by microarray (**Fig. 5A**).

4   Transduced astrocytes were collected by fluorescence-activated cell sorting (FACS) based on

5   their GFP expression. GFP⁻ cells, comprising microglia, neurons, oligodendrocyte precursor cells

6   (OPC), oligodendrocytes and few non-infected astrocytes, were collected together. There were

7   1,415 differentially expressed transcripts (fold change > 1.5, $p < 0.05$), between GFP⁺ and GFP⁻

8   cell samples in control WT-GFP mice (**Fig. 5B**). Besides *eGfp*, many known astrocyte gene

9   markers were enriched in GFP⁺ cells (e.g. *AldoC, Aqp4, Gja1, Gjb6, Slc1a2, Slc1a3*).

10   Conversely, known markers for microglial cells, neurons, OPC, oligodendrocytes were enriched

11   in GFP⁻ cells (e.g. *Aif, Trem2, P2ry12, Pde10a, Snap25, Pdgfra, Myt1*). The sorting procedure

12   being validated, we next compared the gene expression profile of GFP⁺ astrocytes isolated from

13   WT-GFP and WT-JAK2ca mice.

14   Astrocyte samples from these two groups clustered separately by principal component

15   analysis (Fig. **5C**). We found 888 probes (802 unique transcripts) differentially expressed

16   between JAK2ca-astrocytes and control GFP-astrocytes, including *Jak2* mRNA itself

17   (**Supplementary Fig. 2F**). A Gene Ontology (GO) analysis revealed a significant enrichment in

18   many GO-biological processes linked to immunity and inflammation, confirming that JAK2ca

19   triggers reactive changes in astrocytes, which were also evidenced by morphological changes

20   (**Supplementary Fig. 2A-H**)[39].

21   Among the differentially expressed genes between GFP- and JAK2ca-astrocytes, there was a

22   specific enrichment in biological processes linked to lysosomes and UPS, as well as other

23   processes related to proteostasis (**Fig. 5D**). KEGG pathway analysis also revealed a significant

24   enrichment in the term "lysosome" in JAK2ca-reactive astrocytes ($p = 0.0005$). Several

25   cathepsins (*Ctsc, Ctss* and *Ctsz*) were upregulated by JAK2ca in astrocytes (**Fig. 5D**). Genes

26   linked to proteostasis formed a complex network of co-regulated genes in JAK2ca-astrocytes

27   (**Fig. 5D**).

28   To confirm that the JAK2-STAT3 pathway was also able to induce a proteostasis gene signature

29   in astrocytes in a Huntington's disease context, we sorted striatal astrocytes from Hdh140-GFP

30   and Hdh140-JAK2ca mice based on their GFP expression, and performed RNAseq analysis (**Fig.**

13

5E). Again, sorted astrocytes expressed high levels of astrocyte-specific genes and low or undetectable levels of known markers for microglia, neurons, cells of the oligodendrocyte lineage and endothelial cells (**Supplementary Fig. 2I**). Principal component analysis showed that astrocytes from Hdh140-GFP and Hdh140-JAK2ca mice formed two distinct clusters (**Fig. 5F**). We found 269 genes differentially expressed between Hdh140-GFP and Hdh140-JAK2ca astrocytes. *Jak2* levels were significantly higher in JAK2ca-astrocytes than GFP-astrocytes (**Supplementary Fig. 2J**). Murine *Htt,* on the contrary, was expressed at low levels in sorted astrocytes from both groups (rpkm value = 1.859 and 2.120 for GFP- and JAK2ca-astrocytes; adjusted *p*-value = 0.999), showing that JAK2ca does not change *Htt* transcription in striatal astrocytes. Among the 269 differentially expressed genes in Hdh140-JAK2ca astrocytes, 212 genes were present in the full list of 30,845 unique probes detected by microarray analysis of WT striatal astrocytes (i.e. striatal astrocyte transcriptome). And among these 212 genes, only 20 (10%) were also differentially expressed in WT-JAK2ca astrocytes compared to WT-GFP astrocytes. However there was a significant convergence on the functions of the differentially expressed genes between the two studies. In particular, many of the differentially expressed genes in Hdh-140-JAK2ca astrocytes were linked to immunity/inflammation, as found in WT-JAK2ca astrocytes (**Supplementary Fig. 2E**). Likewise, as in WT-JAK2ca astrocytes, there was a significant enrichment in GO pathways related to proteostasis, including the molecular function "Heat shock protein binding" and the cellular components "lytic vacuole" and "lysosome" (**Fig. 5G**). Gene Set Enrichment Annotation (GSEA) also identified the term "phagosome", as significantly enriched in Hdh140-JAK2ca astrocytes, with a majority of up-regulated genes (normalized enrichment score = 1.759, adjusted *p* value = 0.039). Globally, we found that 53% of GO molecular functions, 71% of GO cellular components and 67% of GO biological processes were shared between Hdh140-JAK2ca astrocytes and WT-JAK2ca astrocytes (**Fig. 5H**).

Overall, this transcriptomic analysis shows that JAK2ca induces a specific proteostasis gene signature in striatal astrocytes both in WT and Hdh140 mice.

JAK2ca increases proteolytic capacity in Huntington's disease astrocytes

It is important to establish that the identified transcriptional changes translate into detectable changes in astrocyte function[53]. To assess proteolytic activity of the two major clearance

1 pathways specifically in astrocytes of Huntington's disease mice, we used cell-permeable,

2 activity probes for the lysosomal enzymes cathepsins and for the proteasome (**Supplementary**

3 **Fig. 1B**).

4 We incubated acutely dissociated striatal cells from Hdh140-GFP and Hdh140-JAK2ca mice

5 in a pan-cathepsin activity probe that becomes fluorescent when metabolized by cathepsins[54].

6 We then measured probe fluorescence in GFP[+] astrocytes from the two groups by FACS (**Fig.**

7 **6A**). There was a significantly larger fraction of GFP[+] astrocytes with high cathepsin activity in

8 Hdh140-JAK2ca mice (**Fig. 6B**), revealing that JAK2ca increases lysosomal activity in

9 astrocytes.

10 Another fluorescent probe was used to measure proteasome activity in acutely dissociated

11 astrocytes (**Fig. 6C**)[55]. As the excitation/emission spectrum of this probe overlaps with GFP, we

12 used a viral vector encoding the red fluorescent protein Td-Tomato instead of GFP to detect

13 astrocytes in both groups. Again, the fraction of Td-Tomato[+] astrocytes with high proteasome

14 activity was larger in Hdh140-JAK2ca mice than in Hdh140-Td-Tomato mice (**Fig. 6C**),

15 showing that reactive astrocytes also have a higher proteasome activity.

16 As several ubiquitin ligases were differentially expressed in JAK2ca-astrocytes (**Fig. 5D**), we

17 assessed ubiquitination by immunoblotting striatal homogenates with a Ub antibody. We did not

18 observe major changes in the pattern of Ub immunoreactivity or in total Ub levels between

19 Hdh140-GFP and Hdh140-JAK2ca mice, both in Tx- and SDS-soluble fractions (**Fig. 6D, E**),

20 suggesting that only the proteolytic step of the UPS is stimulated by JAK2ca, without global

21 changes in the ubiquitination profile of mouse striatum.

22 To directly measure the intrinsic capacity of astrocytes to clear mHTT, we used viral vectors

23 to force mHTT expression in astrocytes (LV$_A$-mHTT). WT mice were injected in the right

24 striatum with LV$_A$-mHTT, LV$_A$-SOCS3, and LV$_A$-GFP, and in the control left striatum with

25 LV$_A$-mHTT and LV$_A$-GFP, at the same total viral titer (**Fig. 6F**). Expression of mHTT in

26 astrocytes also triggered STAT3 activation, as evidenced by its nuclear accumulation, and

27 induced reactive changes in astrocytes_(**Fig. 6G**)[8]. In this model as well, SOCS3 efficiently

28 reduced GFAP levels (**Fig. 6G, H**), STAT3 nuclear accumulation (**Fig. 6G, I**) and astrocyte

29 soma hypertrophy (**Fig. 6G, J**). If the JAK2-STAT3 pathway enhances proteolytic activity in

15

1 astrocytes, we reasoned that blocking this pathway with SOCS3 would increase mHTT

2 aggregation in astrocytes. Indeed, we observed that the total number of mHTT aggregates in the

3 striatum was increased with SOCS3 (**Fig. 6K, L**). Moreover, SOCS3 increased mHTT aggregate

4 size (**Fig. 6K, M**). In this model, mHTT forms both nuclear and cytoplasmic inclusions in

5 astrocytes (**Fig. 6K**). The fraction of nuclear aggregates in GFP$^+$ astrocytes was not changed by

6 SOCS3 (19.1% and 22.0% respectively in GFP and SOCS3 groups, Student *t*-test on *arcsine*-

7 transformed data, $n = 6$/group, $df = 5$, $t = 0.787$, $p = 0.458$). These results show that the JAK2-

8 STAT3 pathway stimulates astrocyte intrinsic capacity for mHTT clearance.

JAK2ca induces chaperone expression in astrocytes

10   Interestingly, several GO-molecular functions linked to chaperones and protein folding were

11 significantly regulated by JAK2ca both in WT and Hdh140 astrocytes (**Fig. 5D, G**). Chaperones

12 prevent mHTT aggregation[32, 56] and can be released extracellularly in exosomes[57].

13   We focused on the co-chaperone DNAJB1 [DnaJ heat shock protein family (Hsp40) member

14 B1], a member of the HSP40 family, which is induced nearly 3-fold by JAK2ca in WT astrocytes

15 (**Fig. 5D**). DNAJB1 immunoreactivity was higher in the putamen of Huntington's disease

16 patients, specifically at the core of the degenerative area devoid of NeuN$^+$ neurons and with

17 abundant hypertrophic GFAP$^+$ astrocytes (**Fig. 7A**).

18   JAK2ca significantly increased DNAJB1 protein levels in the striatum of Hdh140 mice as

19 seen by immunostaining (**Fig. 7B, D**) and immunoblotting (**Fig. 7C**), while *Dnajb1* mRNA

20 levels were significantly reduced by SOCS3 in the lentiviral model of Huntington's disease (**Fig.**

21 **7E**). In Hdh140 mice, DNAJB1 displayed a diffuse cytosolic staining but also formed small

22 nuclear inclusion-like structures, suggesting that DNJAB1 can be in close association with

23 mHTT aggregates (**Fig. 7D**).

24   We next studied whether DNAJB1 was found in exosomes and whether DNAJB1 exosomal

25 content was impacted by JAK2-STAT3 activation in Hdh140 mice. Exosomal vesicles were

26 isolated by biochemical fractionation from the striatum of Hdh140-GFP and Hdh140-JAK2ca

27 mice, and they did contain DNAJB1 (**Supplementary Fig. 1C**). DNAJB1 normalized levels

28 displayed a strong tendency to be higher in exosomes of Hdh140-JAK2ca mice than in Hdh140-

29 GFP control mice ($p = 0.056$, **Fig. 7F**).

16

To assess whether DNAJB1 released by JAK2ca-astrocytes contributes to reduce mHTT aggregation in neurons, we generated viral vectors targeting astrocytes and encoding a dominant-negative form of human *DNAJB1* (DNAJB1-DN), which prevents DNAJB1 interaction with the HSP70 chaperone[42], without impacting its loading into exosomes[57]. DNAJB1-DN was expressed in astrocytes in Hdh140-JAK2ca and Hdh140-GFP mice (**Fig. 8A**). DNAJB1-DN, detected by its V5 tag, was confirmed to be expressed in striatal GFP$^+$ astrocytes, throughout their cell body and fine processes (**Fig. 8B**). Interestingly, small V5$^+$ cytoplasmic vesicles were also observed (although rarely) in nearby DARPP32$^+$ neurons (**Fig. 8C**). Some vesicles were co-labelled with the endo-lysosomal marker LAMP1 (**Supplementary Fig. 1D**), suggesting that DNAJB1 can indeed be shuttled from astrocytes to neurons through exosomes. JAK2ca was still able to increase GFAP levels in Hdh140 astrocytes in presence of DNAJB1-DN (**Fig. 8D**). However, co-expression of DNAJB1-DN blocked JAK2ca-mediated reduction of EM48$^+$ aggregate numbers (**Fig. 8E**) and even decreased *Ppp1r1b* mRNA levels (**Fig. 8F**).

Conversely, we tested whether DNAJB1 restoration was able to oppose SOCS3 detrimental effects in the lentiviral model of mHTT overexpression. In the striatum of WT mice, we injected a viral vector targeting astrocytes and encoding a full length human *DNAJB1* (LV$_A$-DNAJB1) with LV$_A$-SOCS3 or LV$_A$-GFP together with LV$_N$-mHTT (**Fig. 8G**). DNAJB1 did not interfere with SOCS3-mediated reduction of GFAP levels in Huntington's disease astrocytes (**Fig. 8H**). However, when DNAJB1 was expressed in astrocytes, SOCS3 no longer exacerbated mHTT aggregation (**Fig. 8I**), neuronal lesion (**Fig. 8J**), or reduced *Ppp1r1b* mRNA levels (**Fig. 8K**), suggesting that DNAJB1 expression in astrocytes counteracts SOCS3 deleterious effects.

Our results suggest that the co-chaperone DNAJB1 produced by JAK2-STAT3 reactive astrocytes helps reduce mHTT aggregation and neuronal alterations in Huntington's disease.

Discussion

*We studied how the JAK2-STAT3 pathway shapes the proteostasis response of reactive astrocytes in Huntington's disease. We found that STAT3 is activated in reactive astrocytes of Huntington's disease patients. T*hanks to two complementary mouse models of Huntington's disease allowing the selective and reciprocal manipulation of the JAK2-STAT3 pathway in striatal astrocytes, we show that this cascade controls astrocyte reactive state and reduces both

17

the number and size of mHTT aggregates forming in neurons.

The reduction of mHTT aggregation by JAK2-STAT3 pathway activation in astrocytes is not due to lower mHTT expression, as *Htt* mRNA levels and Tx-soluble mHTT concentrations were not reduced by JAK2ca. Importantly, JAK2ca-mediated reduction in mHTT aggregation did not trigger an increase in soluble mHTT levels either. This observation rules out that JAK2ca prevents mHTT from coalescing into aggregates or favours the accumulation of soluble mHTT after its dissociation from aggregates. Instead, activation of the JAK2-STAT3 pathway in reactive astrocytes appears to promote the full degradation of mHTT insoluble oligomers or aggregates, which could be mediated by autophagy-lysosomal removal of aggregates or chaperone-mediated extraction of mHTT and targeting to the UPS for complete clearance.

In keeping with this, transcriptomic analysis of acutely sorted astrocytes following JAK2-STAT3 pathway activation in WT and Huntington's disease mice reveals extensive changes in genes linked to lysosomal degradation and the UPS. This result is in accordance with the single nuclei RNAseq analysis of astrocytes from the cingulate cortex of grade III/IV Huntington's disease patients, reporting a significant enrichment in proteostasis functions[5]. Lysosomes and UPS are active in all brain cells and changes in expression or activity in astrocytes could be masked by larger changes in other cell-types if assessed in typical bulk analyses. We thus implemented two FACS-based assays to measure cathepsin and proteasome activity specifically in astrocytes. We found that JAK2ca increases both proteolytic activities in Huntington's disease astrocytes. In addition, our ability to induce mHTT expression selectively in astrocytes by viral gene transfer provides a direct demonstration that the JAK2-STAT3 pathway increases reactive astrocyte capacity to clear mHTT.

As aggregates mainly form in neurons, trans-cellular signalling mechanisms must take place between neurons and reactive astrocytes (**Fig. 8L**). Can mHTT be transferred from neurons to reactive astrocytes where they would be degraded more efficiently? In a landmark study in *Drosophila*, it was shown that mHTT exon 1 tagged with mCherry shuttles from neurons to neighbouring phagocytic glia and forms aggregates with endogenous HTT in glia[58]. Other studies showed that mHTT can be exchanged between brain cells in *Drosophila*, in mice[59-61], and even in humans as mHTT aggregates were detected in healthy embryonic neurons grafted in the brain of Huntington's disease patients[62]. mHTT can be packaged in exosomes of different cell

18

types[63, 64] and be taken up by neighbouring cells, including neurons. Exchange of mHTT may also involve direct cell-to-cell contacts via tunnelling nanotubes[65] or unconventional secretory pathways[66]. Most studies were performed *in vitro* or in non-neuronal cells, therefore, the precise mechanisms of mHTT exchange from neurons to astrocytes in the mammalian brain remain to be elucidated. Of note, a recent study showed that astrocyte-specific silencing of mHTT in a genetic mouse model of Huntington's disease reduces both astrocyte and neuronal mHTT aggregates[20], further supporting the concept of a tight partnership between these two cell types to degrade mHTT.

An alternative and non-exclusive mechanism for reduced neuronal mHTT aggregation upon JAK2-STAT3 pathway activation in astrocytes, is that reactive astrocytes release proteins that promote mHTT clearance within neurons (**Fig. 8L**). Our transcriptomic study shows that several chaperones are induced by JAK2ca in reactive astrocytes. In particular, *DNAJB1* protein levels were higher in Hdh140-JAK2ca mice and this co-chaperone was abundant in extracellular exosomes, and in the lesioned striatum of Huntington's disease patients. Chaperones are known to be released in exosomes and mediate trans-cellular proteostasis[34, 57]. Moreover, exosomes isolated from cultured astrocytes were shown to reduce mHTT aggregation in mice[18]. *Interestingly, single nuclei RNAseq shows that DNAJB1, as well as other chaperones are significantly overexpressed in astrocytes from the* cingulate cortex *of* grade III/IV Huntington's disease *patients*[5] and the putamen of grade II/III patients[9], *showing that this beneficial proteostasis response may also occur in astrocytes from Huntington's disease patients.*

Through *its J domain, DNAJB1 interacts with HSP70 to* stimulate its ATP-dependent chaperone activity[67]. This domain is also implicated in *DNAJB1* loading into exosomes[42, 57]. The J domain alone cannot activate HSP70 and has a dominant-negative action on the endogenous DNAJB1[42]. Expression of this mutant in astrocytes abrogated JAK2ca-mediated beneficial effects in Hdh140 mice, showing DNAJB1 involvement in JAK2ca effects. Conversely, expression of DNAJB1 in astrocytes cancelled SOCS3 deleterious effects on neuronal death and transcriptional defects in the lentiviral model. Small vesicles of tagged DNAJB1 were sometimes observed in neurons nearby infected astrocytes, further supporting the shuttling of DNAJB1 from astrocytes to neurons. Overall, our data strongly suggest that DNAJB1, produced by reactive astrocytes following JAK2-STAT3 pathway activation, promotes mHTT clearance.

19

DNAJB1 was shown to be the rate-limiting chaperone to suppress aggregation of a short fragment of mHtt[68]. Interestingly, HSPs not only prevent mHTT aggregation but can also solubilize proteins trapped in aggregates like transcription factors and favour mHTT degradation by addressing to the UPS or autophagy-lysosomes[33, 69]. Of note, DNAJB1 was recently shown to promote α-synuclein disaggregation[70]. HSP-mediated extraction of housekeeping proteins or mHTT itself from aggregates is expected to reduce their size, which is consistent with our observations. Therefore, HSPs have multiple actions that can *in fine* protect neurons against mHTT toxicity, as shown in different experimental systems based on HSP overexpression[71-73]. Here, we show that neurons rely on the endogenous production of chaperones by astrocytes to reduce mHTT aggregation.

The toxicity of mHTT aggregates is still discussed[24, 69, 74] and mHTT aggregates could have a biphasic action[75]. At early stages, they could trap soluble toxic mHTT and prevent its deleterious interaction with key cellular partners. Later, mHTT aggregates could be detrimental by sequestering transcription factors, housekeeping proteins or microRNAs, leading to neuronal dysfunction and necrotic death[24, 76]. It is important to note that most studies were based on *in vitro* systems allowing time-lapse monitoring of aggregates, but which cannot fully replicate the complex brain environment where neurons interact with multiple glial cells and cope with mHTT for months, and even decades in patients. Here, in two complementary mouse models of Huntington's disease, we report that reduced mHTT aggregation is associated with improved neuronal features, showing that the JAK2-STAT3 pathway shapes a beneficial reactive response in striatal astrocytes. Thanks to sensitive magnetic resonance imaging approaches, we also demonstrate that this pathway reduces striatal atrophy and increases glutamate levels, which are two clinically-relevant disease hallmarks, observed at early stage in patients[49, 50]. Interestingly, we found that the JAK2-STAT3 pathway is still able to activate a protective proteostatic program in Huntington's disease astrocytes. However, the endogenous activation of the JAK2-STAT3 pathway observed in striatal astrocytes from patients seems to be an insufficient protective response to fully prevent neurodegeneration. Early and widespread stimulation of this astrocytic pathway could enhance neuronal resilience in patients.

In conclusion, we show that the JAK2-STAT3 pathway activates a beneficial proteostasis program in reactive astrocytes, which helps striatal neurons handle toxic mHTT. Our study

20

uncovers two non-mutually exclusive, bi-cellular mechanisms to reduce mHTT aggregation in neurons in Huntington's disease (**Fig. 8L**). The first mechanism relies on mHTT exit from neurons and clearance within reactive astrocytes and the second involves the release of chaperones from reactive astrocytes to promote neuronal proteostasis. Astrocytes are not only defective in Huntington's disease as usually reported, they may also acquire enhanced capacities to promote mHTT clearance and neuronal functions, following activation of specific signalling cascades. Our results open new therapeutic avenues to further enhance the natural partnership between reactive astrocytes and vulnerable neurons in Huntington's disease.

Acknowledgements

Funding

1 benefited from Imagerie- Gif core facility supported by French National Research Agency

2 (ANR-11-EQPX-0029/Morphoscope, ANR-10-INBS-04/FranceBioImaging; ANR- 11- IDEX-

3 0003- 02/ Saclay Plant Sciences).

Competing interests

5 The authors declare no competing interests.

Author contribution

7 LA, CE: conception; LA, LBH, MACS, CE: design of the work; LA, LBH, PG, MACS, CD,

8 MAP, FP, ASH, MG, MGG, GA, MK, JF: acquisition of data; LA, LBH, MRP, PG, NS, CH,

9 NR, PdlG, JF, RO: analysis of data; LA, LBH, MRP, JF, EBo, SB, RO, EBr, MACS, CE:

10 interpretation of data; MCG, ND, RM, APB, GB: Provided reagents or materials; JFD, PH, EBr,

11 CE: Provided funding; LA, CE: manuscript writing. All authors revised and approved the

12 manuscript.

Supplementary material

14 Supplementary material is available at *Brain* online.

15

16

References

1. Tabrizi SJ, Flower MD, Ross CA & Wild EJ. Huntington disease: new insights into molecular pathogenesis and therapeutic opportunities. *Nature reviews. Neurology.* 2020; 16, 529-546.

2. TheHuntingtonstudygroup. A novel gene containing a trinucleotide repeat that is expanded and unstable on Huntington's disease chromosomes. The Huntington's Disease Collaborative Research Group. *Cell.* 1993; 72, 971-983.

3. DiFiglia M, Sapp E, Chase KO*, et al.* Aggregation of huntingtin in neuronal intranuclear inclusions and dystrophic neurites in brain. *Science.* 1997; 277, 1990-1993.

4. Jansen AH, van Hal M, Op den Kelder IC*, et al.* Frequency of nuclear mutant huntingtin inclusion formation in neurons and glia is cell-type-specific. *Glia.* 2017; 65, 50-61.

5. Al-Dalahmah O, Sosunov AA, Shaik A*, et al.* Single-nucleus RNA-seq identifies Huntington disease astrocyte states. *Acta neuropathologica communications.* 2020; 8, 19.

6. Vonsattel JP, Myers RH, Stevens TJ, Ferrante RJ, Bird ED & Richardson EP, Jr. Neuropathological classification of Huntington's disease. *Journal of neuropathology and experimental neurology.* 1985; 44, 559-577.

7. Selkoe DJ, Salazar FJ, Abraham C & Kosik KS. Huntington's disease: changes in striatal proteins reflect astrocytic gliosis. *Brain Res.* 1982; 245, 117-125.

8. Faideau M, Kim J, Cormier K*, et al.* In vivo expression of polyglutamine-expanded huntingtin by mouse striatal astrocytes impairs glutamate transport: a correlation with Huntington's disease subjects. *Hum Mol Genet.* 2010; 19, 3053-3067.

9. Lee H, Fenster RJ, Pineda SS*, et al.* Cell Type-Specific Transcriptomics Reveals that Mutant Huntingtin Leads to Mitochondrial RNA Release and Neuronal Innate Immune Activation. *Neuron.* 2020; 107, 891-908 e898.

10. Verkhratsky A & Nedergaard M. Physiology of Astroglia. *Physiological reviews.* 2018; 98, 239-389.

11. Khakh BS, Beaumont V, Cachope R, Munoz-Sanjuan I, Goldman SA & Grantyn R. Unravelling and Exploiting Astrocyte Dysfunction in Huntington's Disease. *Trends Neurosci.* 2017; 40, 422-437.

12. Lievens JC, Woodman B, Mahal A*, et al.* Impaired glutamate uptake in the R6 Huntington's disease transgenic mice. *Neurobiol Dis.* 2001; 8, 807-821.

13. Tong X, Ao Y, Faas GC*, et al.* Astrocyte Kir4.1 ion channel deficits contribute to neuronal dysfunction in Huntington's disease model mice. *Nat Neurosci.* 2014; 17, 694-703.

14. Hsiao HY, Chen YC, Huang CH*, et al.* Aberrant astrocytes impair vascular reactivity in Huntington disease. *Ann Neurol.* 2015; 78, 178-192.

15. Rebec GV, Barton SJ & Ennis MD. Dysregulation of ascorbate release in the striatum of behaving mice expressing the Huntington's disease gene. *J Neurosci.* 2002; 22, RC202.

16. Hong Y, Zhao T, Li XJ & Li S. Mutant Huntingtin Impairs BDNF Release from Astrocytes by Disrupting Conversion of Rab3a-GTP into Rab3a-GDP. *J Neurosci.* 2016; 36, 8790-8801.

17. Wojtowicz AM, Dvorzhak A, Semtner M & Grantyn R. Reduced tonic inhibition in striatal output neurons from Huntington mice due to loss of astrocytic GABA release through GAT-3. *Frontiers in neural circuits.* 2013; 7, 188.

18. Hong Y, Zhao T, Li XJ & Li S. Mutant Huntingtin Inhibits alphaB-Crystallin Expression and Impairs Exosome Secretion from Astrocytes. *J Neurosci.* 2017; 37, 9550-9563.

19. Yu X, Nagai J, Marti-Solano M*, et al.* Context-Specific Striatal Astrocyte Molecular Responses Are Phenotypically Exploitable. *Neuron.* 2020.

20. Diaz-Castro B, Gangwani MR, Yu X, Coppola G & Khakh BS. Astrocyte molecular signatures in Huntington's disease. *Science translational medicine.* 2019; 11.

21. Ceyzériat K, Abjean L, Carrillo-de Sauvage MA, Ben Haim L & Escartin C. The complex STATes of astrocyte reactivity: How are they controlled by the JAK-STAT3 pathway? *Neuroscience.* 2016; 330, 205-218.

22. Ben Haim L, Ceyzeriat K, Carrillo-de Sauvage MA*, et al.* The JAK/STAT3 pathway is a common inducer of astrocyte reactivity in Alzheimer's and Huntington's diseases. *J Neurosci.* 2015; 35, 2817-2829.

23. Schaffar G, Breuer P, Boteva R*, et al.* Cellular toxicity of polyglutamine expansion proteins: mechanism of transcription factor deactivation. *Molecular cell.* 2004; 15, 95-105.

24. Hosp F, Gutierrez-Angel S, Schaefer MH*, et al.* Spatiotemporal Proteomic Profiling of Huntington's Disease Inclusions Reveals Widespread Loss of Protein Function. *Cell reports.* 2017; 21, 2291-2303.

25. Arrasate M, Mitra S, Schweitzer ES, Segal MR & Finkbeiner S. Inclusion body formation reduces levels of mutant huntingtin and the risk of neuronal death. *Nature.* 2004; 431, 805-810.

26. Ortega Z & Lucas JJ. Ubiquitin-proteasome system involvement in Huntington's disease. *Frontiers in molecular neuroscience.* 2014; 7, 77.

27. Cortes CJ & La Spada AR. The many faces of autophagy dysfunction in Huntington's disease: from mechanism to therapy. *Drug discovery today.* 2014; 19, 963-971.

28. Tydlacka S, Wang CE, Wang X, Li S & Li XJ. Differential activities of the ubiquitin-proteasome system in neurons versus glia may account for the preferential accumulation of misfolded proteins in neurons. *J Neurosci.* 2008; 28, 13285-13295.

29. Zhao T, Hong Y, Yin P, Li S & Li XJ. Differential HspBP1 expression accounts for the greater vulnerability of neurons than astrocytes to misfolded proteins. *Proc Natl Acad Sci U S A.* 2017; 114, E7803-E7811.

30. Jansen AH, Reits EA & Hol EM. The ubiquitin proteasome system in glia and its role in neurodegenerative diseases. *Frontiers in molecular neuroscience.* 2014; 7, 73.

31. Sung K & Jimenez-Sanchez M. Autophagy in Astrocytes and its Implications in Neurodegeneration. *Journal of molecular biology.* 2020; 432, 2605-2621.

32. Koyuncu S, Fatima A, Gutierrez-Garcia R & Vilchez D. Proteostasis of Huntingtin in Health and Disease. *International journal of molecular sciences.* 2017; 18.

33. Ciechanover A & Kwon YT. Protein Quality Control by Molecular Chaperones in Neurodegeneration.

Frontiers in neuroscience. 2017; 11, 185.

34. San Gil R, Ooi L, Yerbury JJ & Ecroyd H. The heat shock response in neurons and astroglia and its role in neurodegenerative diseases. *Molecular neurodegeneration.* 2017; 12, 65.

35. Menalled LB, Sison JD, Dragatsis I, Zeitlin S & Chesselet MF. Time course of early motor and neuropathological anomalies in a knock-in mouse model of Huntington's disease with 140 CAG repeats. *J Comp Neurol.* 2003; 465, 11-26.

36. Colin A, Faideau M, Dufour N*, et al.* Engineered lentiviral vector targeting astrocytes in vivo. *Glia.* 2009; 57, 667-679.

37. Naldini L, Blomer U, Gage FH, Trono D & Verma IM. Efficient transfer, integration, and sustained long-term expression of the transgene in adult rat brains injected with a lentiviral vector. *Proc Natl Acad Sci U S A.* 1996; 93, 11382-11388.

38. Lee Y, Messing A, Su M & Brenner M. GFAP promoter elements required for region-specific and astrocyte-specific expression. *Glia.* 2008; 56, 481-493.

39. Ceyzeriat K, Ben Haim L, Denizot A*, et al.* Modulation of astrocyte reactivity improves functional deficits in mouse models of Alzheimer's disease. *Acta neuropathologica communications.* 2018; 6, 104.

40. Guillemaud O, Ceyzériat K, Saint-Georges T*, et al.* Complex roles for reactive astrocytes in the triple transgenic mouse model of Alzheimer disease. *Neurobiol Aging.* 2020; 90, 135-146

41. de Almeida LP, Ross CA, Zala D, Aebischer P & Deglon N. Lentiviral-mediated delivery of mutant huntingtin in the striatum of rats induces a selective neuropathology modulated by polyglutamine repeat size, huntingtin expression levels, and protein length. *J Neurosci.* 2002; 22, 3473-3483.

42. Michels AA, Kanon B, Bensaude O & Kampinga HH. Heat shock protein (Hsp) 40 mutants inhibit Hsp70 in mammalian cells. *J Biol Chem.* 1999; 274, 36757-36763.

43. Hickey MA, Kosmalska A, Enayati J*, et al.* Extensive early motor and non-motor behavioral deficits are followed by striatal neuronal loss in knock-in Huntington's disease mice. *Neuroscience.* 2008; 157, 280-295.

44. Trottier Y, Lutz Y, Stevanin G*, et al.* Polyglutamine expansion as a pathological epitope in Huntington's disease and four dominant cerebellar ataxias. *Nature.* 1995; 378, 403-406.

45. Lunkes A, Lindenberg KS, Ben-Haiem L*, et al.* Proteases acting on mutant huntingtin generate cleaved products that differentially build up cytoplasmic and nuclear inclusions. *Molecular cell.* 2002; 10, 259-269.

46. Pérot JB, Célestine M, Palombo M*, et al.* Identification of the key role of white matter alteration in the pathogenesis of Huntington's Disease. *BioRXiv. In revision at Human Molecular Genetics.* 2021.

47. Chopra V, Quinti L, Khanna P*, et al.* LBH589, A Hydroxamic Acid-Derived HDAC Inhibitor, is Neuroprotective in Mouse Models of Huntington's Disease. *J Huntingtons Dis.* 2016; 5, 347-355.

48. Pepin J, Francelle L, Carrillo-de Sauvage MA*, et al.* In vivo imaging of brain glutamate defects in a knock-in mouse model of Huntington's disease. *Neuroimage.* 2016; 139, 53-64.

49. Wijeratne PA, Garbarino S, Gregory S*, et al.* Revealing the Timeline of Structural MRI Changes in

1 Premanifest to Manifest Huntington Disease. *Neurol Genet.* 2021; 7, e617.

2 50. Adanyeguh IM, Monin ML, Rinaldi D*, et al.* Expanded neurochemical profile in the early stage of Huntington
3 disease using proton magnetic resonance spectroscopy. *NMR Biomed.* 2018; 31.

4 51. Cai K, Haris M, Singh A*, et al.* Magnetic resonance imaging of glutamate. *Nat Med.* 2012; 18, 302-306.

5 52. Pepin J, de Longprez L, Trovero F, Brouillet E, Valette J & Flament J. Complementarity of gluCEST and (1) H-
6 MRS for the study of mouse models of Huntington's disease. *NMR Biomed.* 2020; 33, e4301.

7 53. Escartin C, Galea E, Lakatos A*, et al.* Reactive astrocyte nomenclature, definitions, and future directions. *Nat*
8 *Neurosci.* 2021; 24, 312-325.

9 54. Withana NP, Garland M, Verdoes M, Ofori LO, Segal E & Bogyo M. Labeling of active proteases in fresh-
10 frozen tissues by topical application of quenched activity-based probes. *Nature protocols.* 2016; 11, 184-
11 191.

12 55. Berkers CR, van Leeuwen FW, Groothuis TA*, et al.* Profiling proteasome activity in tissue with fluorescent
13 probes. *Mol Pharm.* 2007; 4, 739-748.

14 56. Hartl FU, Bracher A & Hayer-Hartl M. Molecular chaperones in protein folding and proteostasis. *Nature.*
15 2011; 475, 324-332.

16 57. Takeuchi T, Suzuki M, Fujikake N*, et al.* Intercellular chaperone transmission via exosomes contributes to
17 maintenance of protein homeostasis at the organismal level. *Proc Natl Acad Sci U S A.* 2015; 112, E2497-
18 2506.

19 58. Pearce MM, Spartz EJ, Hong W, Luo L & Kopito RR. Prion-like transmission of neuronal huntingtin
20 aggregates to phagocytic glia in the Drosophila brain. *Nature communications.* 2015; 6, 6768.

21 59. Pecho-Vrieseling E, Rieker C, Fuchs S*, et al.* Transneuronal propagation of mutant huntingtin contributes to
22 non-cell autonomous pathology in neurons. *Nat Neurosci.* 2014; 17, 1064-1072.

23 60. Babcock DT & Ganetzky B. Transcellular spreading of huntingtin aggregates in the Drosophila brain. *Proc*
24 *Natl Acad Sci U S A.* 2015; 112, E5427-5433.

25 61. Donnelly KM, DeLorenzo OR, Zaya AD*, et al.* Phagocytic glia are obligatory intermediates in transmission of
26 mutant huntingtin aggregates across neuronal synapses. *Elife.* 2020; 9.

27 62. Cicchetti F, Lacroix S, Cisbani G*, et al.* Mutant huntingtin is present in neuronal grafts in Huntington disease
28 patients. *Ann Neurol.* 2014; 76, 31-42.

29 63. Diaz-Hidalgo L, Altuntas S, Rossin F*, et al.* Transglutaminase type 2-dependent selective recruitment of
30 proteins into exosomes under stressful cellular conditions. *Biochim Biophys Acta.* 2016; 1863, 2084-2092.

31 64. Jeon I, Cicchetti F, Cisbani G*, et al.* Human-to-mouse prion-like propagation of mutant huntingtin protein.
32 *Acta Neuropathol.* 2016; 132, 577-592.

33 65. Costanzo M, Abounit S, Marzo L*, et al.* Transfer of polyglutamine aggregates in neuronal cells occurs in
34 tunneling nanotubes. *J Cell Sci.* 2013; 126, 3678-3685.

35 66. Trajkovic K, Jeong H & Krainc D. Mutant Huntingtin Is Secreted via a Late Endosomal/Lysosomal

1   Unconventional Secretory Pathway. *J Neurosci.* 2017; 37, 9000-9012.

2   67.   Kampinga HH & Craig EA. The HSP70 chaperone machinery: J proteins as drivers of functional specificity.

3   *Nature reviews. Molecular cell biology.* 2010; 11, 579-592.

4   68.   Scior A, Buntru A, Arnsburg K*, et al.* Complete suppression of Htt fibrilization and disaggregation of Htt

5   fibrils by a trimeric chaperone complex. *EMBO J.* 2018; 37, 282-299.

6   69.   Mogk A, Bukau B & Kampinga HH. Cellular Handling of Protein Aggregates by Disaggregation Machines.

7   *Molecular cell.* 2018; 69, 214-226.

8   70.   Wentink AS, Nillegoda NB, Feufel J*, et al.* Molecular dissection of amyloid disaggregation by human HSP70.

9   *Nature.* 2020; 587, 483-488.

10   71.   Popiel HA, Takeuchi T, Fujita H*, et al.* Hsp40 gene therapy exerts therapeutic effects on polyglutamine

11   disease mice via a non-cell autonomous mechanism. *PLoS One.* 2012; 7, e51069.

12   72.   Warrick JM, Chan HY, Gray-Board GL, Chai Y, Paulson HL & Bonini NM. Suppression of polyglutamine-

13   mediated neurodegeneration in Drosophila by the molecular chaperone HSP70. *Nature genetics.* 1999; 23,

14   425-428.

15   73.   Bason M, Meister-Broekema M, Alberts N*, et al.* Astrocytic expression of the chaperone DNAJB6 results in

16   non-cell autonomous protection in Huntington's disease. *Neurobiol Dis.* 2019; 124, 108-117.

17   74.   Arrasate M & Finkbeiner S. Protein aggregates in Huntington's disease. *Exp Neurol.* 2012; 238, 1-11.

18   75.   Ramdzan YM, Trubetskov MM, Ormsby AR*, et al.* Huntingtin Inclusions Trigger Cellular Quiescence,

19   Deactivate Apoptosis, and Lead to Delayed Necrosis. *Cell reports.* 2017; 19, 919-927.

20   76.   Pircs K, Petri R, Madsen S*, et al.* Huntingtin Aggregation Impairs Autophagy, Leading to Argonaute-2

21   Accumulation and Global MicroRNA Dysregulation. *Cell reports.* 2018; 24, 1397-1406.

22

23

Figure legends

Figure 1. **STAT3 nuclear accumulation in the putamen of Huntington's disease patients**

STAT3 immunoreactivity is higher in the putamen of Huntington's disease patients (**B, C**) than in control subjects (**A**), especially in regions displaying many hypertrophic GFAP$^+$ astrocytes, and major neurodegeneration, as seen with the loss NeuN staining (**C**). STAT3 is often found accumulated in the nucleus of cells with a typical astrocyte morphology (arrows and high magnification in **B** and **C**). Representative images from 4 subjects/group.

Figure 2. **JAK2ca induces astrocyte reactivity and reduces neuronal mHTT aggregation in Hdh140 mice**

A. Hdh140 mice (7-9 month-old) were injected in the striatum with LV$_A$-GFP or LV$_A$-JAK2ca + LV$_A$-GFP, at the same total virus load, and their brains analysed 4 months later. **B.** Low magnification images (left) show the GFP$^+$ transduced area (outlined, green) and GFAP staining (magenta) in the striatum of Hdh140-GFP and Hdh140-JAK2ca mice. High magnification images (right) of astrocytes stained for GFP (green), GFAP (magenta), and STAT3 (cyan). JAK2ca triggers STAT3 activation, as seen by its nuclear accumulation, increases GFAP and vimentin levels and induces morphological changes in astrocytes. Note that the basal expression of GFAP is nearly undetectable in Hdh140 mice, suggesting very mild reactive changes in this model. **C, D.** GFAP$^+$ volume (**C**) and soma area of GFP$^+$ astrocytes (**D**) are significantly increased by JAK2ca. Student *t*-test. *n* = 3-5/group, *df* = 5, **C**: *t* = 8.081, *p* = 0.0005; **D**: *t* = 4.703, *p* = 0.0053. **E, F.** JAK2ca increases *Vimentin* (**E**) and *Serpina3n* (**F**) mRNA levels. Student *t*-test. *n* = 3-5/group, *df* = 5, **E**: *t* = 2.917, *p* = 0.0331; **F**: *t* = 3.748, *p* = 0.0133. **G.** Bright field images of EM48$^+$ aggregates in the striatum of Hdh140-GFP and Hdh140-JAK2ca mice. The striatal region displaying EM48$^+$ aggregates is outlined on low magnification images. **H, I.** Total number (**H**) and size (**I**) of EM48$^+$ aggregates are significantly decreased by JAK2ca in the striatum of Hdh140 mice. Student *t*-test. *n* = 3-5/group, *df* = 5, **H**: *t* = 6.606, *p* = 0.0012; **I**: *t* = 3.142, *p* = 0.0256. **J.** Confocal images of striatal sections stained for GFP (green), EM48 (white) and DARPP32 (magenta). EM48$^+$ aggregates are mostly found in neurons labelled with DARPP32 (arrowhead) and very rarely in GFP$^+$ astrocytes (green, arrow). **K**. JAK2ca decreases the total number of EM48$^+$ aggregates, but the distribution of EM48$^+$ aggregates between GFP$^+$ astrocytes and DARPP32$^+$ neurons is not changed. **L, M.** Immunoblotting on the Tx-soluble

1   fraction of mHTT with the 1C2 antibody. Similar levels of mHTT are detected in Hdh140-GFP

2   and Hdh140-JAK2ca mice, while mHTT is undetectable in WT mice. There is no mHTT

3   cleavage fragments detected by this antibody in both Hdh140-GFP and Hdh140-JAK2ca mice.

4   Paired *t*-test, $n = 5$, $df = 4$, $t = 1.845$ $p = 0.139$. **N, O.** Immunoblotting on the SDS-soluble

5   fraction of high molecular weight species (HMW) of mHTT with the 2B4 antibody. JAK2ca

6   decreases the levels of insoluble HMW mHTT species in Hdh140 mice. Band intensity was

7   normalized to actin. Paired *t*-test. $n = 5$/group, $df = 4$, $t = 3.367$, $p = 0.0281$.

8   **Figure 3. SOCS3-inhibition of the JAK2-STAT3 pathway in astrocytes increases the**

9   **number and size of neuronal mHTT aggregates**

10 **A.** Two month-old WT mice were injected with LV_N-mHTT + LV_A-GFP in one striatum and

11 with LV_N-mHTT + LV_A-SOCS3 + LV_A-GFP in the contralateral striatum, at the same total virus

12 load. Their brains were analysed 6 weeks later. **B.** Low magnification images show the

13 transduced GFP$^+$ area (green, outlined) in the striatum and immunostaining for GFAP (magenta).

14 **C.** High magnification confocal images of astrocytes stained for GFP (green), GFAP (magenta)

15 and STAT3 (cyan). **D-F**. Immunoreactivity for GFAP (**D**) and STAT3 (**E**), as well as astrocyte

16 soma area (**F**) are significantly decreased by SOCS3. Paired *t*-test. $n = 5$-6/group, **D**: $df = 5$, $t =$

17 4.349, $p = 0.0074$; **E**: $df = 4$, $t = 8.651$, $p = 0.0010$; **F**: $df = 4$, $t = 2.961$, $p = 0.0415$. **G.** The

18 striatal volume with EM48$^+$ aggregates is significantly increased by SOCS3. Paired *t*-test. $n =$

19 6/group, $df = 5$, $t = 3.096$, $p = 0.0270$. **H.** Confocal images of striatal sections stained for GFP

20 (green), EM48 (white), neurotrace (magenta) and DAPI (blue). Large EM48$^+$ aggregates of

21 mHTT are mostly found in neurons stained for neurotrace, occupying their entire nucleus

22 (arrowhead). Only few GFP$^+$ astrocytes display an EM48$^+$ aggregate (arrow). **I.** Immunolabeling

23 for ubiquitin (Ub) shows Ub$^+$ aggregates in the striatum (delimited with black dots). **J.** The

24 number of Ub$^+$ inclusions is significantly increased by SOCS3. Wilcoxon matched-pair test, $n =$

25 5/group, $p = 0.0431$. **K.** Ub$^+$ inclusions are larger in the striatum injected with LV_A-SOCS3 than

26 LV_A-GFP. Paired *t*-test. $n = 5$/group, $df = 4$, $t = 3.406$, $p = 0.0271$.

27

29

Figure 4. Activation of the JAK2-STAT3 pathway in astrocytes has beneficial effects on striatal neurons

A. Mice were injected as in **Fig. 2A**. Striatal *Ppp1r1b* mRNA levels are higher in Hdh140-JAK2ca mice than in Hdh140-GFP mice. Student *t*-test. n = 3-5/group, df = 5, t = 3.028, p = 0.0291. **B.** T_2-weigthed magnetic resonance images show that LV_A-JAK2ca reduces striatal atrophy in Hdh140 mice. Note the larger ventricle in the side injected with the control vector LV_A-GFP, caused by striatal atrophy (arrow). Wilcoxon matched-pair test, p = 0.0313. **C.** Quantification of gluCEST contrast in Hdh140 mice reveals higher glutamate levels in the striatum injected with LV_A-JAK2ca. Paired *t*-test, n = 6, df = 5, t = 5.641, p = 0.0024. Two representative mice are shown, each on a different anatomical position. Region of interest are shown with black dash on each striatum. **D-F** Mice were injected as in **Fig. 3A**. **D.** Low and high magnification images of striatal sections stained for DARPP32 (red) showing the striatal lesion caused by mHTT, appearing as a an area devoid of DARPP32+ neurons (white dotted lines). **E.** Striatal DARPP32$^-$ lesions are significantly larger in the SOCS3 group. Wilcoxon matched-pair test, n = 6/group, p = 0.0277. **F.** SOCS3 decreases mRNA levels of the neuronal transcripts *Ppp1r1b* (*Darpp32*). Student *t*-test. n = 4-5/group, df = 7, t = 3.931, p = 0.0057.

Figure 5. JAK2ca regulates the expression of proteostasis genes in astrocytes

A. Two month-old WT mice were injected in the striatum with AAV-GFP or AAV-JAK2ca + AAV-GFP (N = 4/group), at the same total virus load. After 2 months, GFP$^+$ striatal astrocytes were acutely sorted and their transcriptome analysed by microarray. **B.** Validation of astrocyte isolation. The volcano plot shows the 1,415 differentially expressed genes between GFP$^+$ astrocytes and GFP$^-$ cells in WT-GFP mice (in green overexpressed in GFP$^+$ cells; in orange, overexpressed in GFP$^-$ cells). eGFP and established cell-type specific markers are shown. GFP$^+$ cells express typical astrocyte markers while GFP$^-$ cells express markers for microglial cells, neurons, cells of the oligodendrocyte lineage and endothelial cells. **C.** Principal component analysis shows a clear segregation of the four WT-GFP and four WT-JAK2ca astrocyte samples. **D**. GO analysis on the list of JAK2ca-regulated genes in GFP$^+$ astrocytes reveals a significant enrichment in several biological processes linked to autophagy/lysosome or UPS and in molecular functions linked to chaperones. Network plot with the genes involved in the selected GO pathways. n = 4/group. **E.** Hdh140 mice (8-10 month-old) were injected in the striatum with

AAV-GFP or AAV-JAK2ca + AAV-GFP, at the same total virus load. After 4 months, GFP$^+$ striatal astrocytes were collected and analysed by RNAseq. **F.** The five Hdh140-GFP samples cluster apart from the six Hdh140-JAK2ca astrocyte samples, on a principal component analysis graph. **G.** GO analysis reveals a significant enrichment in genes involved in molecular functions (MF), cellular components (CC) and biological processes (BP) linked to proteostasis. The x axis represents the ratio of the number of differentially expressed genes over the total number of genes belonging to a GO entry, DEG = differentially expressed genes. n = 5-6/group. **H**. Venn diagrams for the enriched GO molecular functions, cellular components and biological functions, from the list of differentially expressed genes in WT-JAK2ca and Hdh140-JAK2ca astrocytes. There is a majority of common terms.

Figure 6. JAK2ca increases cathepsin and proteasome intrinsic activities in Huntington's disease striatal astrocytes

A-C. The striatum of Hdh-JAK2ca mice and their control Hdh140-GFP or Hdh140-Td-Tomato was collected, cells dissociated and incubated with a quenched fluorescent pan-cathepsin activity probe (**B**) or a proteasome activity probe (**C**). The percentage of GFP$^+$ astrocytes with cathepsin activity (**B**) or the percentage of Td-Tomato$^+$ astrocytes with proteasome activity (**C**) was quantified in each mouse. Hdh140-JAK2ca mice display a higher percentage of astrocytes with cathepsin or proteasome activity. Paired *t*-test on *arcsine*-transformed data. **C**: n = 9/group, df = 8, t = 3.183, p = 0.0129. **D**: n = 7/group, df = 6, t = 6.001, p = 0.0010. **D, E.** Immunoblotting for Ub was performed on striatal Tx-soluble and SDS-soluble fractions from WT-GFP, WT-JAK2ca, Hdh140-GFP and Hdh140-JAK2ca mice. Immunoreactivity pattern and total Ub levels are not different between groups. Band intensity was normalized to α-tubulin. For Tx-soluble: Two-way (genotype, treatment) ANOVA, n = 5-6/group, df = 1, Genotype: F = 0.038, p = 0.8481; Treatment: F = 0.224, p = 0.6421, Genotype x Treatment: F = 0.776, p = 0.3900. For SDS-soluble: Kruskal-Wallis test n = 5-6/group, p = 0.3211. **F-M.** Two month-old WT mice were injected in one striatum with LV$_A$-mHTT and LV$_A$-GFP and the contralateral striatum with LV$_A$-mHTT, LV$_A$-SOCS3 and LV$_A$-GFP (same total viral load) to force mHTT expression in astrocytes. Their brains were analysed 6 weeks later. **G.** Low magnification images showing GFP$^+$ transduced area (outlined, green) and GFAP staining (magenta) in the mouse striatum. Confocal images of striatal sections stained for GFP (green), GFAP (magenta) and STAT3

31

1 (cyan). SOCS3 reduces GFAP immunoreactivity and nuclear accumulation of STAT3 in

2 astrocytes. **H-J**. Quantification of GFAP immunoreactivity (**H**), STAT3 immunoreactivity (**I**)

3 and astrocyte soma area (**J**). SOCS3 significantly decreases all these parameters. **H**: Wilcoxon

4 matched-pair test, $n = 6$/group, $p = 0.0277$. **I**: Paired t-test. $n = 6$/group, $df = 5$, $t = 4.354$, $p =$

5 0.0073. **J**: Paired t-test. $n = 6$/group, $df = 5$, $t = 5.442$, $p = 0.0028$. **K**. Confocal images of striatal

6 sections stained for GFP (green), EM48 (white) and DAPI (blue). Large EM48^{+} aggregates form

7 in astrocyte nucleus (arrow), while small aggregates are mainly found in astrocyte processes

8 (arrowhead). **L, M**. The total number (**L**) and the size (**M**) of EM48^{+} aggregates are significantly

9 increased by SOCS3. Paired t-test. $n = 6$/group, $df = 5$, **L**: $t = 3.246$, $p = 0.0228$. **M**: $t = 2.778$, p

10 $= 0.0390$.

11 **Figure 7. The *JAK2-STAT3 pathway increases DNAJB1* expression in astrocytes**

12 **A.** DNAJB1 display a strong immunoreactivity in the degenerative putamen region that is filled

13 with GFAP[+] astrocytes in Huntington's disease patients. **B, C.** Immunostaining (**B**) and

14 immunoblotting (**C**) show higher DNAJB1 protein levels in the striatum of Hdh140-JAK2ca

15 mice than Hdh140-GFP mice. Band intensity was normalized to α-tubulin. **B**: Student t-test. $n =$

16 3-5/group, $df = 5$, $t = 2.658$, $p = 0.0450$. **C**: Paired t-test. $n = 5$/group, $df = 4$, $t = 4.079$, $p =$

17 0.0151. **D**. Confocal images of striatal sections stained for GFP (green), DNAJB1 (white) and

18 DARPP32 (magenta). DNAJB1 displays a diffuse cytosolic staining and forms small nuclear

19 inclusions in neurons (arrow) of Hdh140 mice. **E.** *Dnajb1* mRNA levels are significantly

20 decreased by SOCS3 in LV$_N$-mHTT mice. Student t-test. $n = 4$-5/group, $df = 7$, $t = 2.525$, $p =$

21 0.0395. **F.** DNAJB1 is present in exosomes isolated from Hdh140 striata and its levels,

22 normalized by stain free staining, tend to be higher in Hdh140-JAK2ca than Hdh140-GFP

23 exosomes. Student t-test. $n = 4$-5/group, $df = 7$, $t = 2.290$, $p = 0.0558$.

24 **Figure 8. DNAJB1 is involved in the anti-aggregation effects of the JAK2-STAT3**

25 **pathway**

26 **A.** Hdh140 mice (8-9 month-old) were injected in one striatum with LV$_A$-GFP + LV$_A$-DNAJB1-

27 DN and with LV$_A$-JAK2ca + LV$_A$-GFP + LV$_A$-DNAJB1-DN in the contralateral striatum, at the

28 same total virus load. Their brains were analysed 4 months later. **B.** Representative confocal

29 images showing striatal sections stained for GFP (green) and V5 (cyan) in astrocytes. **C**. V5[+]

30 vesicles (cyan, arrows) are observed in the cytoplasm of DARPP32^{+} striatal neurons (magenta).

High magnification of a single z plane and orthogonal views are shown on the right, DAPI is shown in blue. Contrary to infected astrocytes expressing high levels of V5 throughout their cytoplasm, including in their fine processes infiltrating the neuropil (arrowheads), neurons display V5 staining only in few cytoplasmic vesicles, ruling out a direct infection of striatal neurons by LV$_A$-DNAJB1-DN. Additional negative controls are shown in **Supplementary Fig. 1D. D.** JAK2ca increases GFAP immunoreactivity in astrocytes overexpressing DNAJB1-DN in Hdh140 mice. Wilcoxon matched-pair test, $n = 8$/group, $p = 0.0077$. **E.** In presence of DNAJB1-DN, the total number of EM48$^+$ aggregates is no longer decreased by JAK2ca. Wilcoxon matched-pair test, $n = 8$/group, $p = 0.7794$. **F.** *Ppp1r1b* mRNA levels are significantly reduced by JAK2ca in Hdh140 mice expressing DNAJB1-DN. Wilcoxon matched-pair test, $n = 8$/group, $p = 0.0431$. **G.** Two month-old WT mice were injected in one striatum with LV$_N$-mHTT + LV$_A$-GFP + LV$_A$-DNAJB1 and the contralateral striatum with LV$_N$-mHTT + LV$_A$-SOCS3 + LV$_A$-DNAJB1, at the same total virus load and analysed 6 weeks later. **H.** SOCS3 reduces GFAP immunoreactivity in LV$_N$-mHTT mice, even in presence of DNJAB1. Paired *t*-test. $n = 9$/group, $df = 8$, $t = 3.534$, $p = 0.0077$. **I.** SOCS3 no longer increases the EM48$^+$ volume when astrocytes co-express DNAJB1. Paired *t*-test. $n = 9$/group, $df = 8$, $t = 2.004$, $p = 0.0851$. **J, K.** Likewise, striatal DARPP32$^-$ lesions (**J**) and *Ppp1r1b* mRNA levels (**K**) are no longer different between the two groups. **J**: Paired *t*-test. $n = 9$/group, $df = 8$, $t = 0.632$, $p = 0.5451$. **K:** Wilcoxon matched-pair test, $n = 8$/group, $p = 0.8203$. **L. Bi-directional communication between JAK2-STAT3-induced reactive astrocytes and neurons to promote proteostasis in Huntington's disease:** The JAK2-STAT3 pathway induces a reactive response in striatal astrocytes and activates a transcriptional program that promotes proteostasis, reduces mHTT aggregation and improves neuronal status. Two complementary and non-exclusive mechanisms involving striatal neurons and JAK2-STAT3-dependent reactive astrocytes may take place. **1.** Reactive astrocytes display a higher intrinsic proteolytic activity that promotes mHTT degradation. Neurons could shuttle their mHTT to astrocytes for clearance. The exact mechanisms and the form of mHTT exchanged (monomers, fibrils, cleaved fragments…) remain to be determined. **2.** Reactive astrocytes over-express chaperones such as DNAJB1 that can be released in exosomes towards neurons to promote their proteostasis.
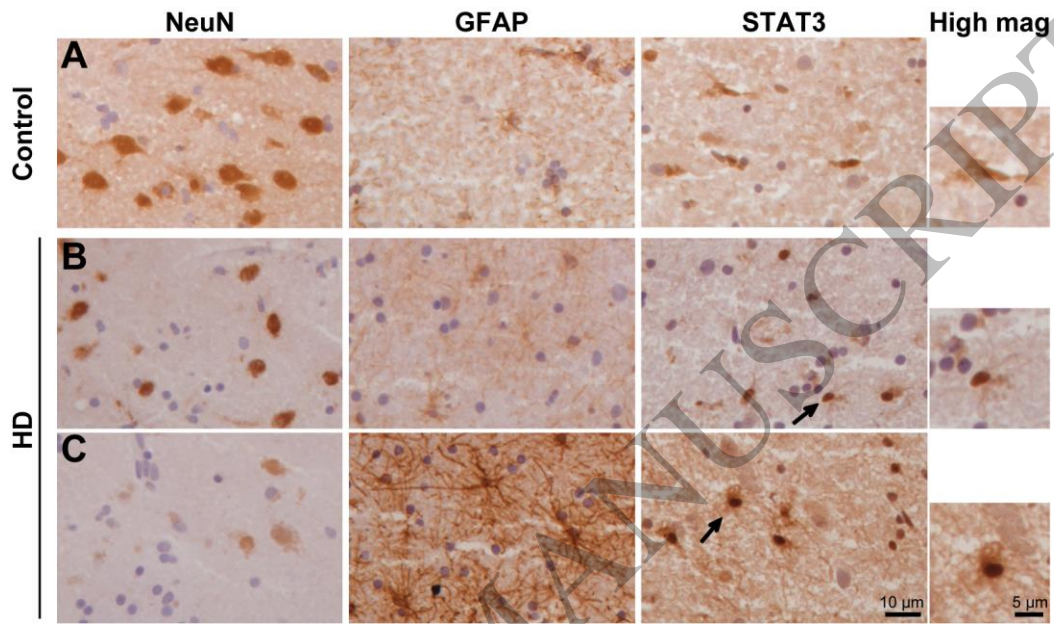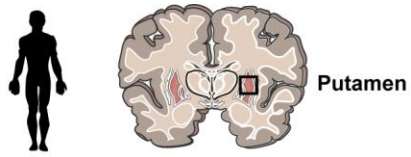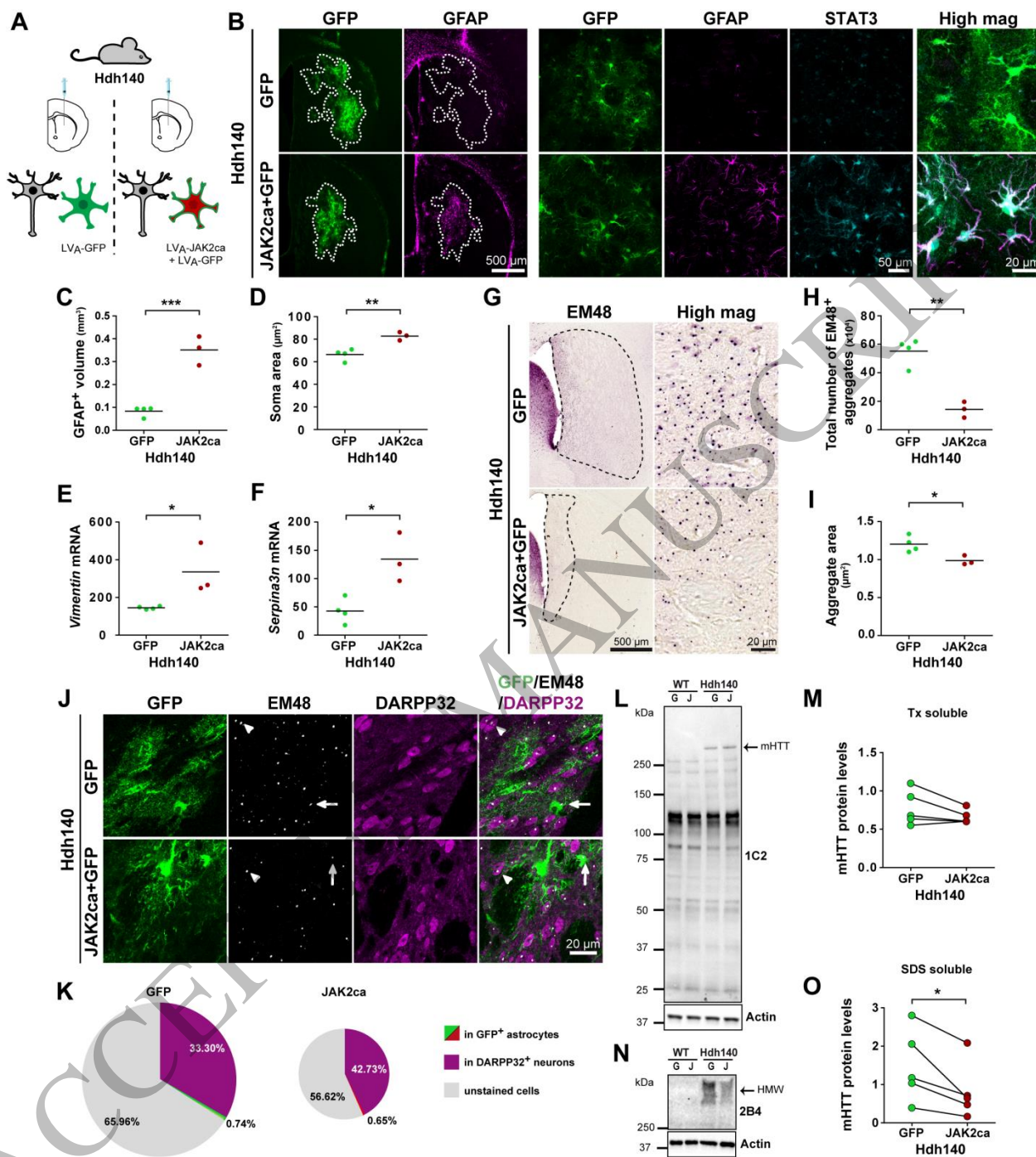
Figure 1
138x107 mm (1.7 x DPI)

Figure 2
209x233 mm (1.7 x DPI)

1

2
3
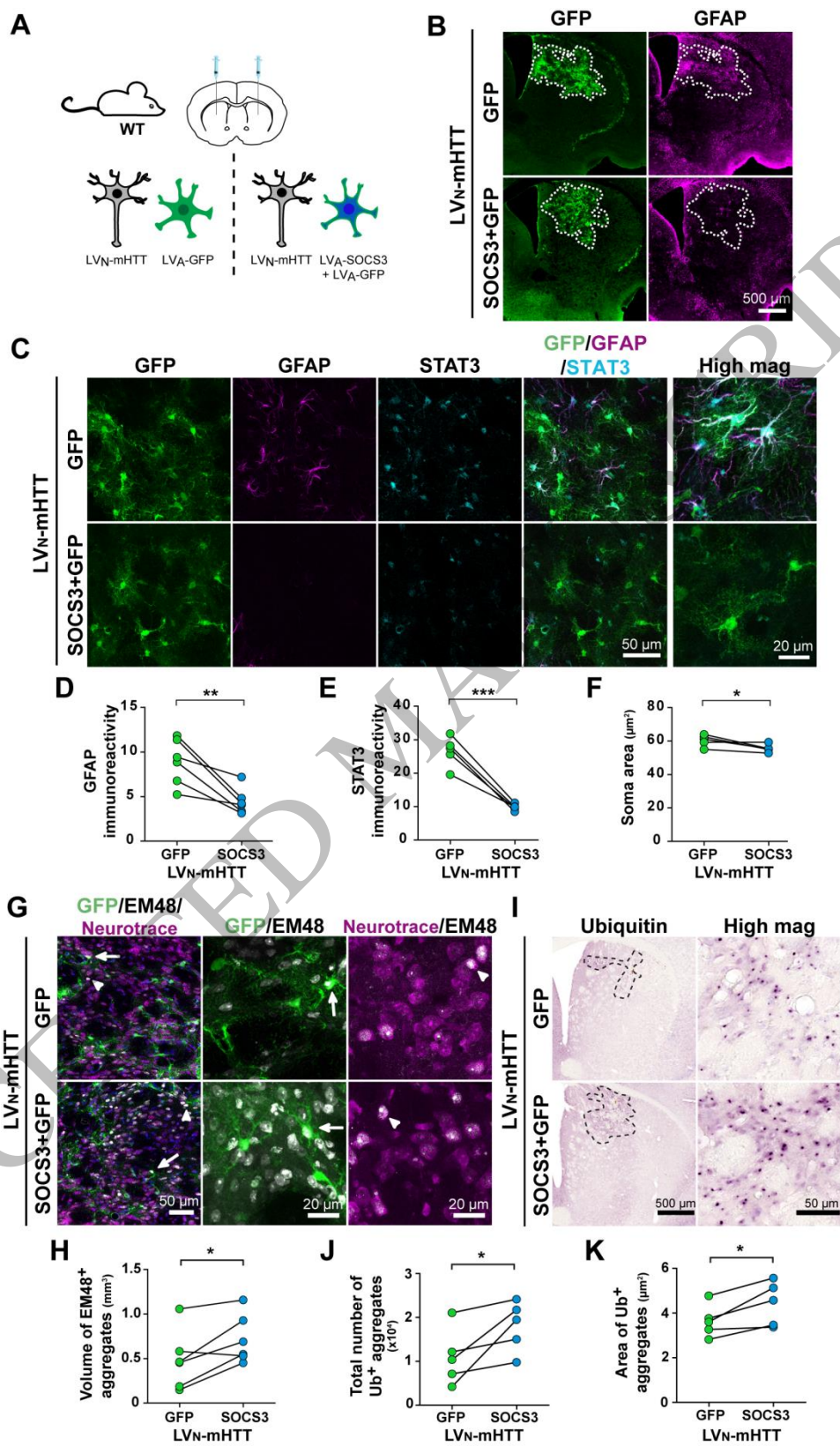
Figure 3
147x251 mm (1.7 x DPI)

1
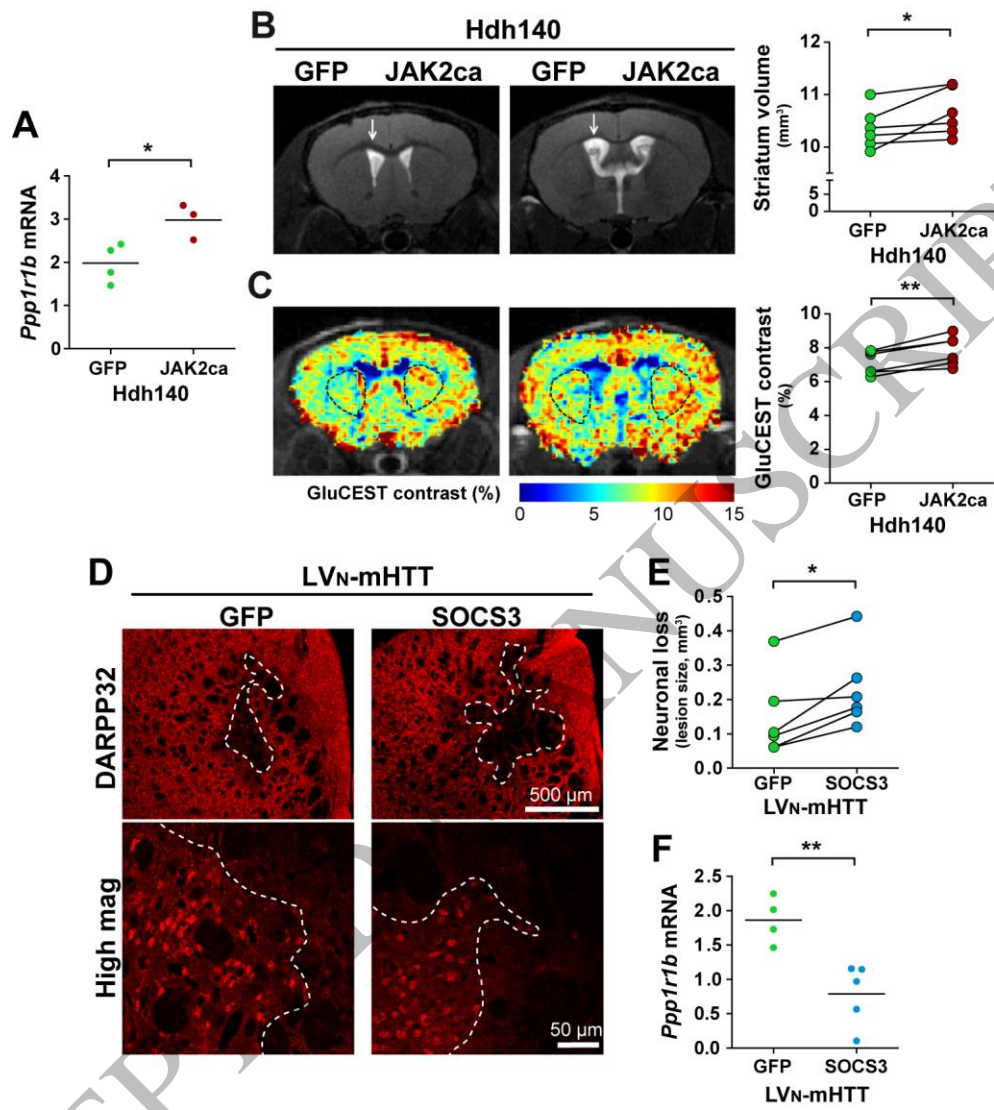
Figure 4
130x146 mm (1.7 x DPI)

2
3
4

5

1
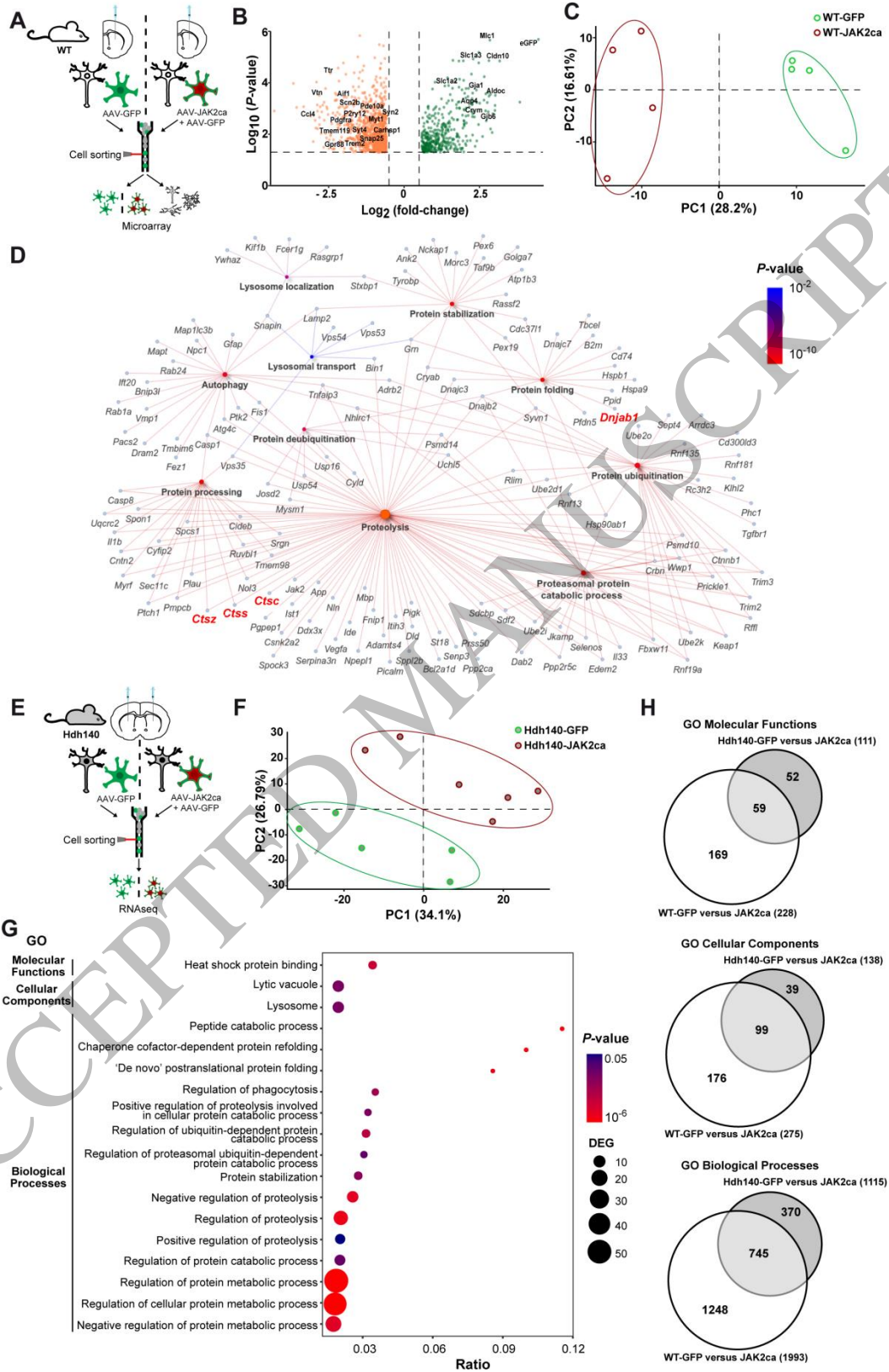
2 **Figure 5**
3 **189x294 mm (1.7 x DPI)**
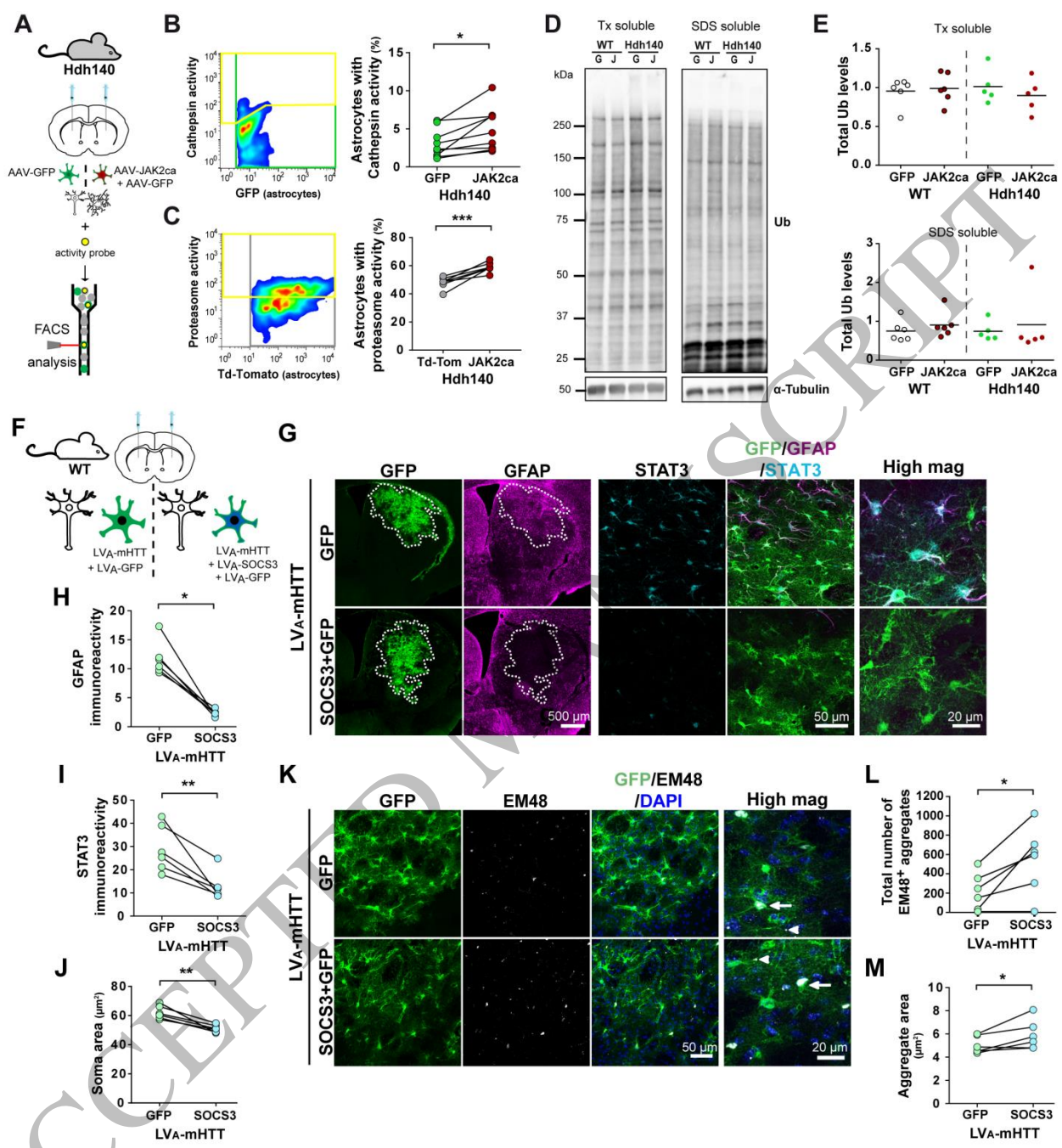
Figure 6
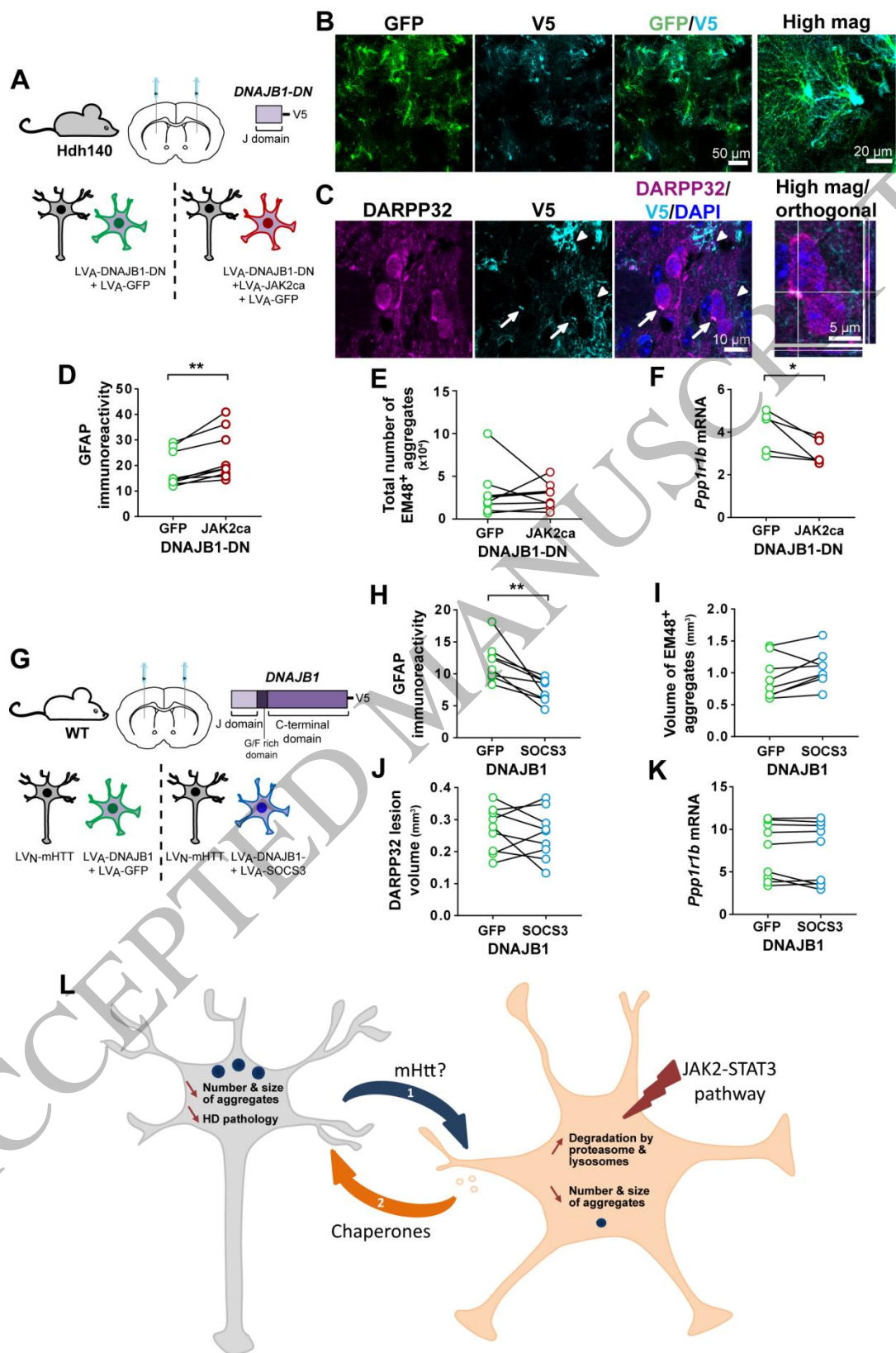**209x223 mm (1.7 x DPI)**

39
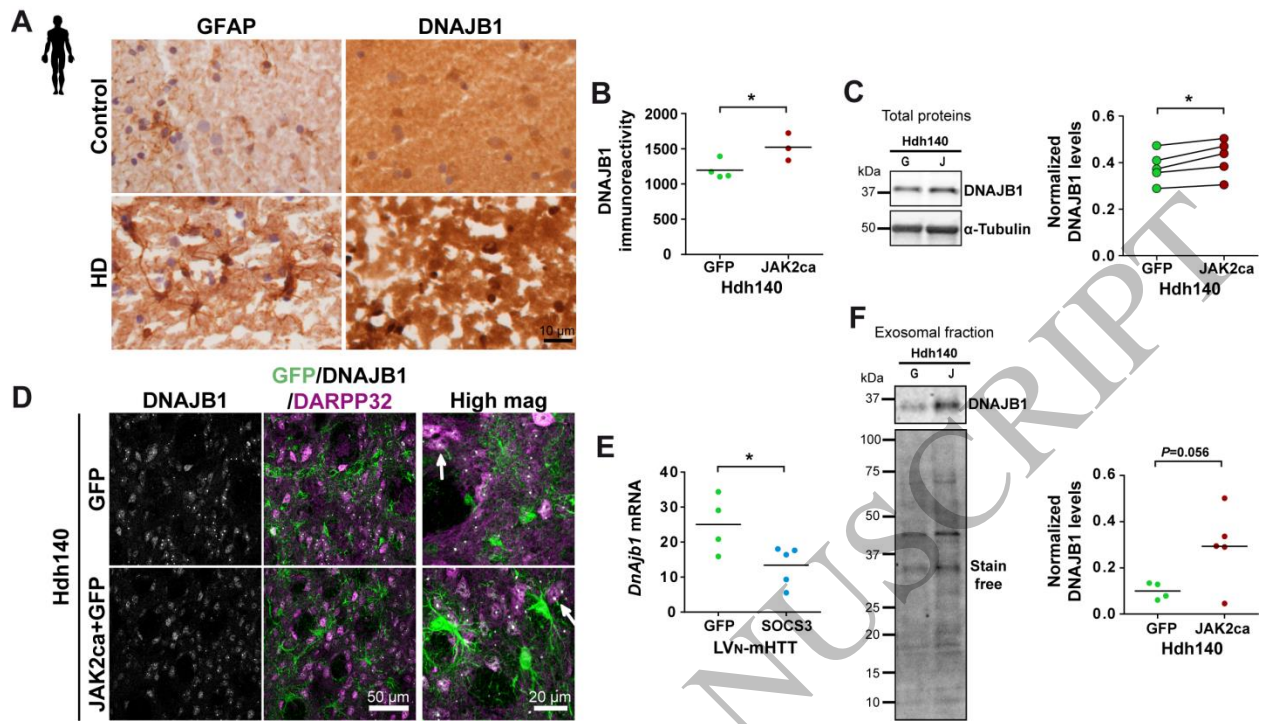
Figure 7
205x117 mm (1.7 x DPI)

Figure 8
161x245 mm (1.7 x DPI)

41